Article

Cancer Cell

Targeting Non-proteolytic Protein Ubiquitination for the Treatment of Diffuse Large B Cell Lymphoma

Highlights

- cIAP1/2 are functional E3 ligases in ABC DLBCL that promote NF-κB activation
- cIAP1/2 reside in the CBM complex and deposit K63-polyubiquitin chains there
- cIAP1/2 help to recruit LUBAC and IκB kinase to the CBM complex
- SMAC mimetics degrade cIAP1/2 and block growth of BCR-dependent ABC DLBCL xenografts

Authors

Yibin Yang, Priscilla Kelly, Arthur L. Shaffer III, ..., Jan Delabie, Lisa Rimsza, Louis M. Staudt

Correspondence

lstaudt@mail.nih.gov

In Brief

Yang et al. show that cIAP1 and cIAP2 mediate K63 ubiquitination of BCL10, thus are essential for B cell receptor (BCR)-dependent NF-κB activity in the ABC subtype of diffuse large B cell lymphoma (DLBCL). SMAC mimetics target cIAP1/2 for destruction, selectively killing BCR-dependent ABC DLBCL cells.

Accession Numbers

GSE73281
GSE73639

Yang et al., 2016, Cancer Cell *29*, 494–507
April 11, 2016
http://dx.doi.org/10.1016/j.ccell.2016.03.006

CellPress

CellPress

Cancer Cell
Article

Targeting Non-proteolytic Protein Ubiquitination for the Treatment of Diffuse Large B Cell Lymphoma

Yibin Yang,[1] Priscilla Kelly,[1] Arthur L. Shaffer III,[1] Roland Schmitz,[1] Hee Min Yoo,[1] Xinyue Liu,[1] Da Wei Huang,[1] Daniel Webster,[1] Ryan M. Young,[1] Masao Nakagawa,[1] Michele Ceribelli,[1] George W. Wright,[2] Yandan Yang,[1] Hong Zhao,[1] Xin Yu,[1] Weihong Xu,[1] Wing C. Chan,[3] Elaine S. Jaffe,[4] Randy D. Gascoyne,[5] Elias Campo,[6] Andreas Rosenwald,[7] German Ott,[8] Jan Delabie,[9] Lisa Rimsza,[10] and Louis M. Staudt[1,*]

[1]Lymphoid Malignancies Branch, Center for Cancer Research, National Cancer Institute, National Institutes of Health, 9000 Rockville Pike, Building 10, Room 4N115, Bethesda, MD 20892, USA
[2]Biometric Research Branch, Division of Cancer Diagnosis and Treatment, National Cancer Institute, National Institutes of Health, Bethesda, MD 20892, USA
[3]Department of Pathology, City of Hope National Medical Center, Duarte, CA 91010, USA
[4]Laboratory of Pathology, Center for Cancer Research, National Cancer Institute, Bethesda, MD 20892, USA
[5]British Columbia Cancer Agency, Vancouver, BC V5Z 4E6, Canada
[6]Hospital Clinic, University of Barcelona, 08036 Barcelona, Spain
[7]Department of Pathology, University of Würzburg, 97080 Würzburg, Germany
[8]Department of Clinical Pathology, Robert-Bosch-Krankenhaus, Dr. Margarete Fischer-Bosch Institute for Clinical Pharmacology, 70376 Stuttgart, Germany
[9]Department of Pathology, University Health Network, Toronto, Ontario M5G 2C4, Canada
[10]Department of Pathology, University of Arizona, Tucson, AZ 85724, USA
*Correspondence: lstaudt@mail.nih.gov
http://dx.doi.org/10.1016/j.ccell.2016.03.006

SUMMARY

Chronic active B cell receptor (BCR) signaling, a hallmark of the activated B cell-like (ABC) subtype of diffuse large B cell lymphoma (DLBCL), engages the CARD11-MALT1-BCL10 (CBM) adapter complex to activate IκB kinase (IKK) and the classical NF-κB pathway. Here we show that the CBM complex includes the E3 ubiquitin ligases cIAP1 and cIAP2, which are essential mediators of BCR-dependent NF-κB activity in ABC DLBCL. cIAP1/2 attach K63-linked polyubiquitin chains on themselves and on BCL10, resulting in the recruitment of IKK and the linear ubiquitin chain ligase LUBAC, which is essential for IKK activation. SMAC mimetics target cIAP1/2 for destruction, and consequently suppress NF-κB and selectively kill BCR-dependent ABC DLBCL lines, supporting their clinical evaluation in patients with ABC DLBCL.

INTRODUCTION

The diffuse large B cell lymphoma (DLBCL) diagnostic category encompasses two molecular subtypes, activated B cell-like (ABC) and germinal center B cell-like (GCB), which are histologically indistinguishable but differ profoundly in their gene expression phenotypes and in the oncogenic genomic variants that they acquire (Shaffer et al., 2012). The ABC subtype was so named because its gene expression profile resembles that of normal B cells in which the B cell receptor (BCR) has been engaged by antigen (Alizadeh et al., 2000). The vast majority of ABC DLBCL primary tumors and cell lines have a gene expression signature that reflects nuclear factor κB (NF-κB) pathway activation, suggesting that this pathway is central to the pathogenesis of this cancer type (Davis et al., 2001). Indeed, functional and structural genomic studies have revealed the molecular mechanisms underlying constitutive NF-κB activity in ABC DLBCL, highlighting the key role of chronic active BCR signaling and oncogenic MYD88 mutations (Davis et al., 2010; Lenz et al., 2008a; Ngo et al., 2011). These molecular insights have led to advances in the treatment of ABC DLBCL, including the effectiveness of ibrutinib, a Bruton's tyrosine kinase (BTK) inhibitor that prevents BCR signaling from engaging the NF-κB pathway (Wilson et al., 2015). The success of ibrutinib in producing

Significance

The present study uncovers a role for the ubiquitin ligases cIAP1 and cIAP2 in the BCR signaling pathway as resident components of the CBM complex. SMAC mimetics, which potently reduce the abundance of cIAP1 and cIAP2, have displayed an acceptable safety profile in clinical trials but have yet to show significant activity against solid tumors. We propose that ABC DLBCL is a superior clinical setting in which to demonstrate the efficacy of SMAC mimetics, since cIAP1 and cIAP2 are integral components of a key oncogenic pathway in this lymphoma subtype.

remissions in ABC DLBCL prompted us to search for additional molecular targets in the BCR pathway that are amenable to therapeutic attack.

Protein ubiquitination regulates NF-κB activation at multiple levels within the various signaling cascades that engage this survival pathway (Chen, 2012). In particular, the K63-linked and linear polyubiquitin chains modulate signaling networks and are required for efficient and fine-tuned NF-κB induction in response to various stimuli (Walczak et al., 2012). The linear ubiquitin chain assembly complex (LUBAC), which joins ubiquitin moieties in a head-to-tail fashion, is required for NF-κB-dependent survival of ABC DLBCL (Yang et al., 2014). In the chronic active BCR signaling that characterizes ABC DLBCL, LUBAC associates with the CARD11-BCL10-MALT1 (CBM) signaling complex, where it attaches linear polyubiquitin to the NEMO (IKKγ) subunit of IκB kinase (IKK), the key regulatory kinase in the NF-κB pathway. However, the mechanism by which the CBM complex recruits and regulates LUBAC function is unknown.

K63-linked ubiquitination controls many aspects of NF-κB signaling by creating binding platforms for proteins that have ubiquitin-binding domains that recognize K63 linkages, such as the LUBAC subunit RNF31 and NEMO (Fujita et al., 2014; Gerlach et al., 2011; Ikeda et al., 2011; Kensche et al., 2012). The cellular inhibitor of apoptosis 1 and 2 (cIAP1 and cIAP2) proteins are E3 ubiquitin ligases that facilitate the attachment of both K63-linked and K48-linked polyubiquitin chains to target proteins (Liston et al., 1996). cIAP1 and cIAP2 (cIAP1/2) belong to the inhibitor of apoptosis protein (IAP) family owing to their three amino-terminal IAP repeat domains, which facilitate binding to caspases and other proteins (Roy et al., 1997; Samuel et al., 2006). In addition, cIAP1/2 have carboxy-terminal RING finger domains that mediate their E3 ubiquitin ligase activities (Yang et al., 2000). Although cIAP1/2 can bind to caspases, they are poor caspase inhibitors (Eckelman and Salvesen, 2006). Instead, cIAP1/2 regulate various signal transduction pathways, including the activation of NF-κB in response to various stimuli (Chu et al., 1997; Park et al., 2004; Rothe et al., 1995; Samuel et al., 2006; Shu et al., 1996; Varfolomeev et al., 2007; Vince et al., 2007; Wang et al., 1998).

Initial evidence that cIAP1/2 regulate the classical NF-κB pathway arose from studies of signaling by tumor necrosis factor alpha (TNF-α) (Micheau and Tschopp, 2003; Rothe et al., 1995). Following TNF receptor I engagement by TNF-α, multiple signaling proteins are recruited to the receptor, including cIAP1/2. The E3 ligase activity of cIAP1/2 is thereby stimulated, leading to K63-linked polyubiquitination of cIAP1/2 themselves and the adapter RIP1. K63-linked polyubiquitin chains are recognized by the ubiquitin-binding domains of various signaling mediators, including the TAB1/2-TAK1 complex and LUBAC (Bertrand et al., 2008; Haas et al., 2009; Varfolomeev et al., 2008).

A second function of cIAP1/2 is to restrain the alternative NF-κB pathway, which was uncovered during the genetic analysis of multiple myeloma (Annunziata et al., 2007; Keats et al., 2007). Subsequent mechanistic investigations revealed that a protein complex consisting of cIAP1/2, TRAF2, and TRAF3 functions in the cytosol to degrade the kinase NIK, an activator of the alternative NF-κB pathway (Vallabhapurapu et al., 2008; Zarnegar et al., 2008b). In the current model, cIAP1/2 are believed to mediate K48 polyubiquitination and degradation of NIK, since deletion of cIAP1/2 results in NIK accumulation. Ligand engagement by certain TNF family receptors recruits cIAP1/2-TRAF2-TRAF3 complex to the receptor, causing cIAP1/2 to instead target TRAF2 and TRAF3 for destruction, thereby stabilizing NIK and activating NF-κB. Deletion of both cIAP1 and cIAP2 in mouse B cells results in expansion of the peripheral B cell pool, apparently due to constitutive activation of the alternative NF-κB pathway (Gardam et al., 2011). Deletion and/or mutation of TRAF3 occurs in ~15% of ABC DLBCL tumors and contributes to alternative NF-κB activation in these cases (Zhang et al., 2015).

A role for cIAP1/2 in B cells participating in adaptive immune responses was revealed by mice lacking expression of cIAP1 and cIAP2 in B cells, which were significantly impaired in their ability to generate a germinal center immune response to a T cell-dependent antigen (Gardam et al., 2011). While this phenotype was ascribed to a defect in CD40 signaling in B cells, the possibility that BCR signaling might be impaired was not tested. Following BCR and T cell receptor (TCR) cross-linking, BCL10 acquires K63-linked polyubiquitin (Satpathy et al., 2015; Wu and Ashwell, 2008), but the responsible K63 ubiquitin ligase has not been reported. In addition, BCL10 is modified with linear polyubiquitin following BCR engagement (Satpathy et al., 2015), which is presumed to be a consequence of LUBAC association with the CBM complex (Yang et al., 2014). Ubiquitination of BCL10 is necessary to efficiently recruit IKK to the CBM complex and activate NF-κB following TCR engagement (Wu and Ashwell, 2008), but the role of BCL10 ubiquitination in BCR-dependent NF-κB activation has not been investigated.

Pharmaceutical efforts to inhibit IAP proteins were inspired by structural and functional analysis of second mitochondria-derived activator of caspases (SMAC), a small protein that is released from mitochondria during apoptosis and inhibits IAP proteins by binding to their BIR domains (Fulda and Vucic, 2012). Small molecules that function like SMAC (SMAC mimetics) have a range of specificities for IAP family members, with some tailored to block XIAP engagement of caspases while others have more specificity for cIAP1/2. Monomeric cIAP1/2 exist in an autoinhibited state in which the RING domain interacts with the BIR3 domain. Certain SMAC mimetics bind to the BIR3 domain, thereby releasing the RING domain to dimerize and become an active E3 ligase, ultimately leading to intense K48-linked autoubiquitination and destruction of the protein (Dueber et al., 2011). One such SMAC mimetic under clinical investigation is birinapant (TL32711), a dimeric molecule with two cIAP1/2 binding moieties that promotes cIAP1/2 degradation and inhibits NF-κB activation by TNF-α in various tumor cell models, thereby promoting tumor cell death (Allensworth et al., 2013; Benetatos et al., 2014; Condon et al., 2014; Krepler et al., 2013).

The role of K63-linked polyubiquitination in pro-survival oncogenic signaling in ABC DLBCL has not been explored in detail. We hypothesized that K63-linked ubiquitination by cIAP1/2 had an important role in ABC DLBCL biology and that cIAP1/2 antagonists may be effective therapeutic agents in this disease.

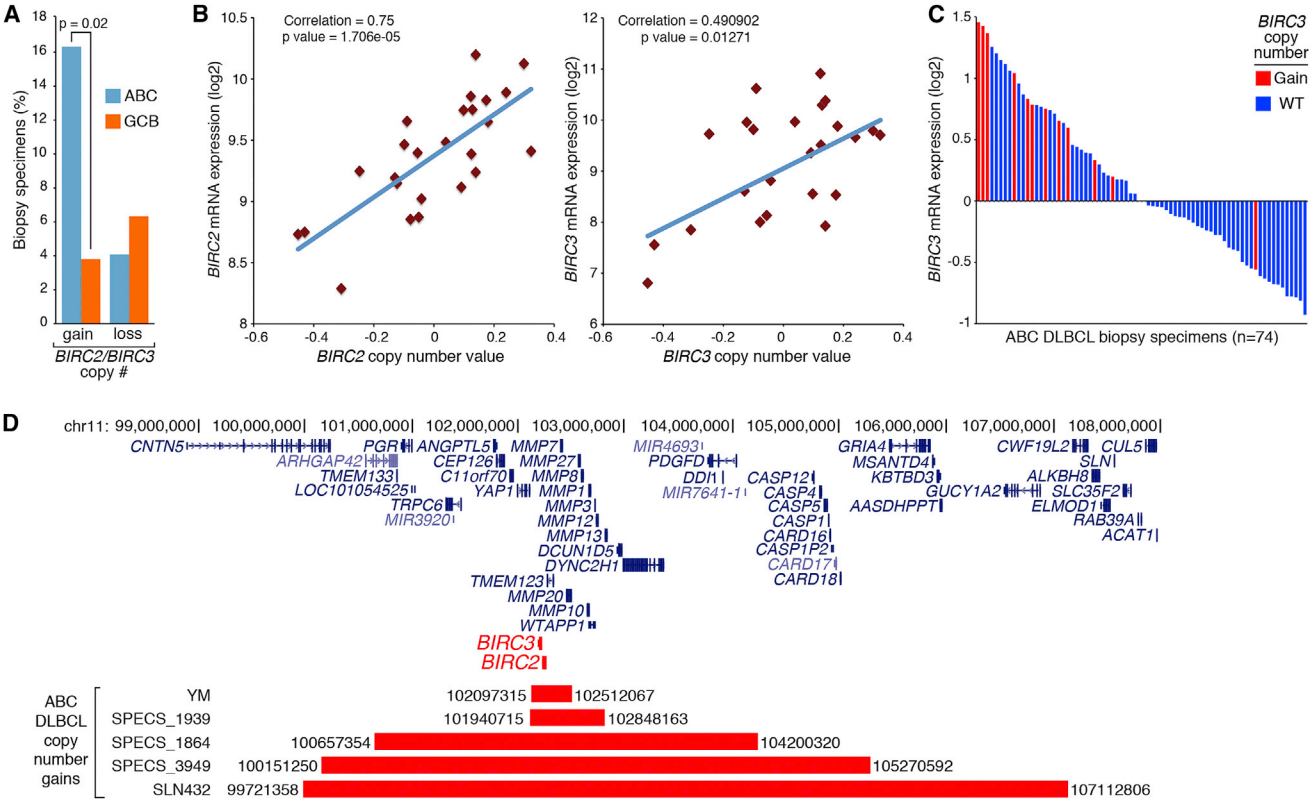

Figure 1. Copy Number Gains of BIRC2/3 Loci in ABC DLBCL Biopsy Specimens

(A) Frequency of *BIRC2*/*BIRC3* copy number changes in ABC and GCB DLBCL cases by aCGH.

(B) Correlation between *BIRC2* (left) or *BIRC3* (right) mRNA levels with gene copy number in DLBCL.

(C) *BIRC3* mRNA levels in 74 ABC DLBCL biopsy specimens.

(D) Chromosomal regions containing *BIRC2* and *BIRC3* with focal copy number gain in ABC DLBCL samples.

See also Figure S1 and Table S1.

RESULTS

Frequent Copy Number Gains of the *BIRC2*/*BIRC3* Locus in ABC DLBCL

The genes encoding cIAP1 and cIAP2, *BIRC2* and *BIRC3*, respectively, are situated next to each other on human chromosome 11. In an array-based comparative genomic hybridization (aCGH) dataset from DLBCL tumors (Scholtysik et al., 2015), gain/amplification of the genomic region encompassing *BIRC2* and *BIRC3* was significantly more common in ABC DLBCL (8 of 49; 16.33%) than in GCB DLBCL (3 of 79, 3.8%) (Figure 1A). By contrast, both ABC and GCB DLBCL tumors had comparably low frequencies of copy number loss of the *BIRC2*/*BIRC3* locus (4.1% versus 6.3%, p = 0.7071). *BIRC2* and *BIRC3* expression levels correlated with DLBCL copy number (Figure 1B). In an independent set of ABC DLBCL (Lenz et al., 2008b), those with *BIRC2*/*BIRC3* copy number gains had high relative *BIRC3* mRNA levels by gene expression profiling (Figure 1C) and real-time PCR (Figure S1). A majority (8 of 11) of ABC DLBCL cases with *BIRC2*/*BIRC3* copy number gains had either an *MYD88* or *CD79B* mutation, while none had mutations affecting CARD11 or A20, which regulate downstream BCR and MYD88 signaling (Table S1). While most of the *BIRC2*/*BIRC3* locus copy number gains encompassed many megabases, aCGH revealed that some were more focal (Figure 1D). One ABC DLBCL cell line, YM, has a copy number gain involving *BIRC2* and *BIRC3* and only three other genes, which is notable since YM cells depend on cIAP1 and cIAP2 for survival (see below). These genetic findings prompted us to explore the role of cIAP1/2 in ABC DLBCL biology.

cIAP1/2 Contribute to Classical NF-κB Activity in ABC DLBCL

To examine the oncogenic role of cIAP1/2 in ABC DLBCL, we used SMAC mimetics to reduce their expression ABC DLBCL lines. All three SMAC mimetics tested, AT-146, birinapant, and SM-164, reduced the protein levels of cIAP1 and cIAP2 in each ABC DLBCL line (Figure S2A). To gain insight into which biological processes were regulated by cIAP1/2 in ABC DLBCL, we compared the gene expression changes caused by birinapant with a database of gene expression signatures that reflect regulatory processes in normal and malignant blood cells (Shaffer et al., 2006). The genes downregulated by birinapant overlapped significantly with signatures reflecting NF-κB signaling in ABC DLBCL (Table S2 and Figure 2A). NF-κB signaling genes were downregulated in three BCR-dependent ABC DLBCL lines (OCI-Ly10, TMD8, and HBL1), but not in the BCR-independent ABC DLBCL line OCI-Ly3. Expression of NF-κB signature genes

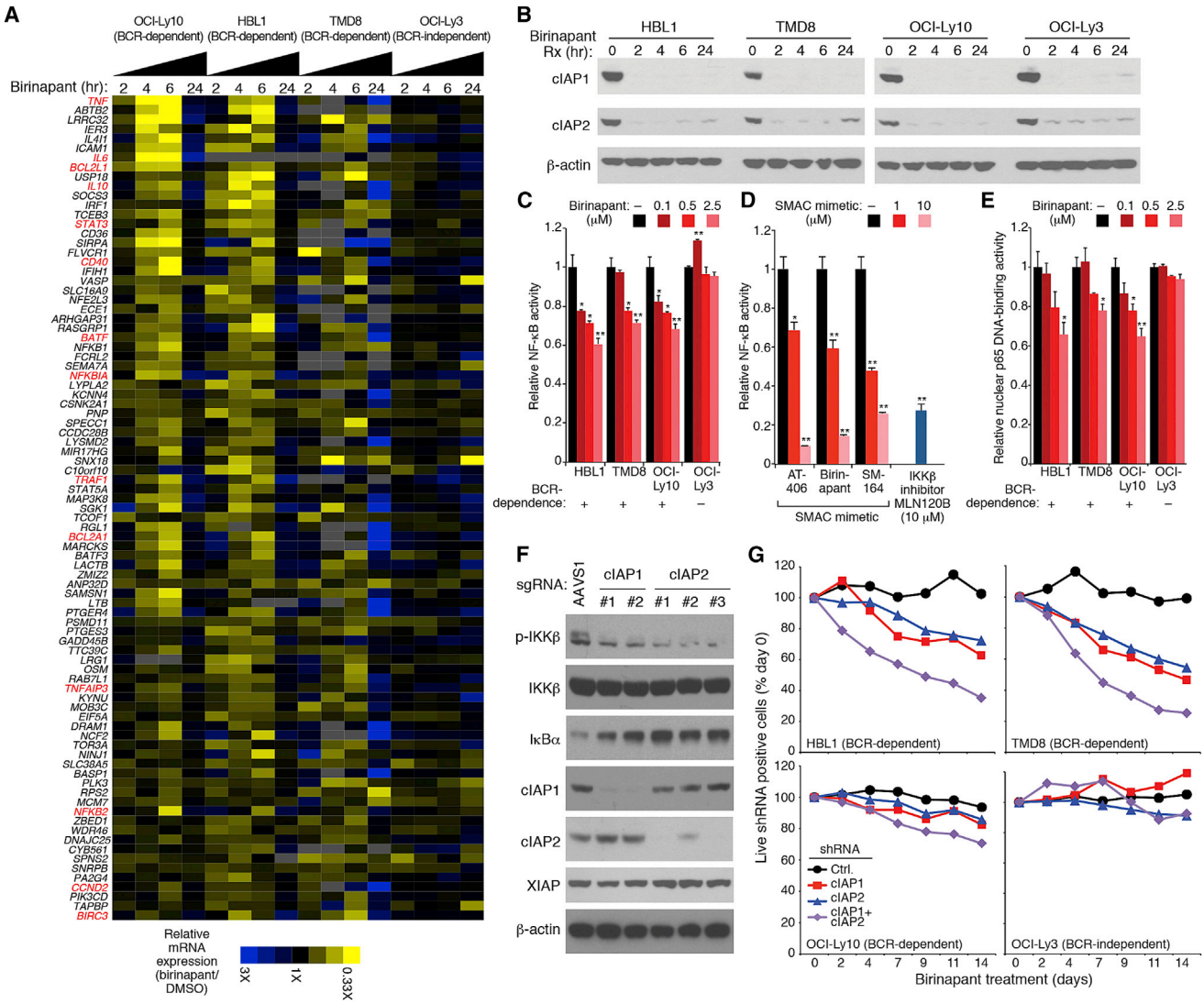

Figure 2. cIAP1/2 Contribute to the Classic NF-κB Activation Pathway in ABC DLBCL

(A) mRNA levels of NF-κB signature genes (Shaffer et al., 2006) in the indicated ABC DLBCL lines treated with birinapant (2.5 μM) relative to DMSO-treated cells.

(B) Immunoblot analysis of the indicated proteins in whole-cell lysates of ABC DLBCL lines treated with birinapant (2.5 μM) for the indicated times.

(C) Relative activity of an NF-κB-dependent luciferase reporter in ABC DLBCL lines after treatment with the indicated birinapant concentrations for 24 hr.

(D) Relative activity of an NF-κB-dependent luciferase reporter in the HBL1 line upon treatment of indicated drugs for 24 hr.

(E) ELISA measurement of relative NF-κB p65 DNA-binding activity in nuclear extracts from ABC DLBCL lines treated with the indicated birinapant concentrations for 24 hr.

(F) Cell lysates from HBL1 cells transduced with lentiviruses expressing the indicated sgRNAs, puromycin selected (5 days), and further cultured (11 days) were immunoblotted for the indicated proteins.

(G) The fraction of viable shRNA-expressing cells relative to the total live-cell fraction at the indicated times following induction of the indicated shRNAs, normalized to day-0 values.

All error bars denote SEM of triplicates. p Values (Student's t test) compare treatment groups with the DMSO control. *$p < 0.05$; **$p < 0.01$. See also Figure S2 and Table S2.

decreased maximally after 6 hr of birinapant treatment but then rebounded at 24 hr, which may be partially explained by a modest rise in cIAP2 protein levels at 24 hr (Figure 2B). However, this rebound in NF-κB target gene expression may also be explained by effects of cIAP1/2 depletion on the alternative NF-κB pathway (see below).

In three BCR-dependent ABC DLBCL lines, but not in the BCR-independent OCI-Ly3 line, birinapant inhibited NF-κB activity in a dose-dependent manner (Figures 2C and S2B). Three structurally distinct SMAC mimetics inhibited the NF-κB reporter and were as effective as MLN120B, a selective IKKβ inhibitor (Lam et al., 2005) (Figure 2D). Treatment of three BCR-dependent ABC DLBCL lines with birinapant decreased the nuclear abundance of NF-κB dimers containing the p65 subunit, indicating that cIAP1/2 contribute to classical NF-κB activity in these cells (Figure 2E).

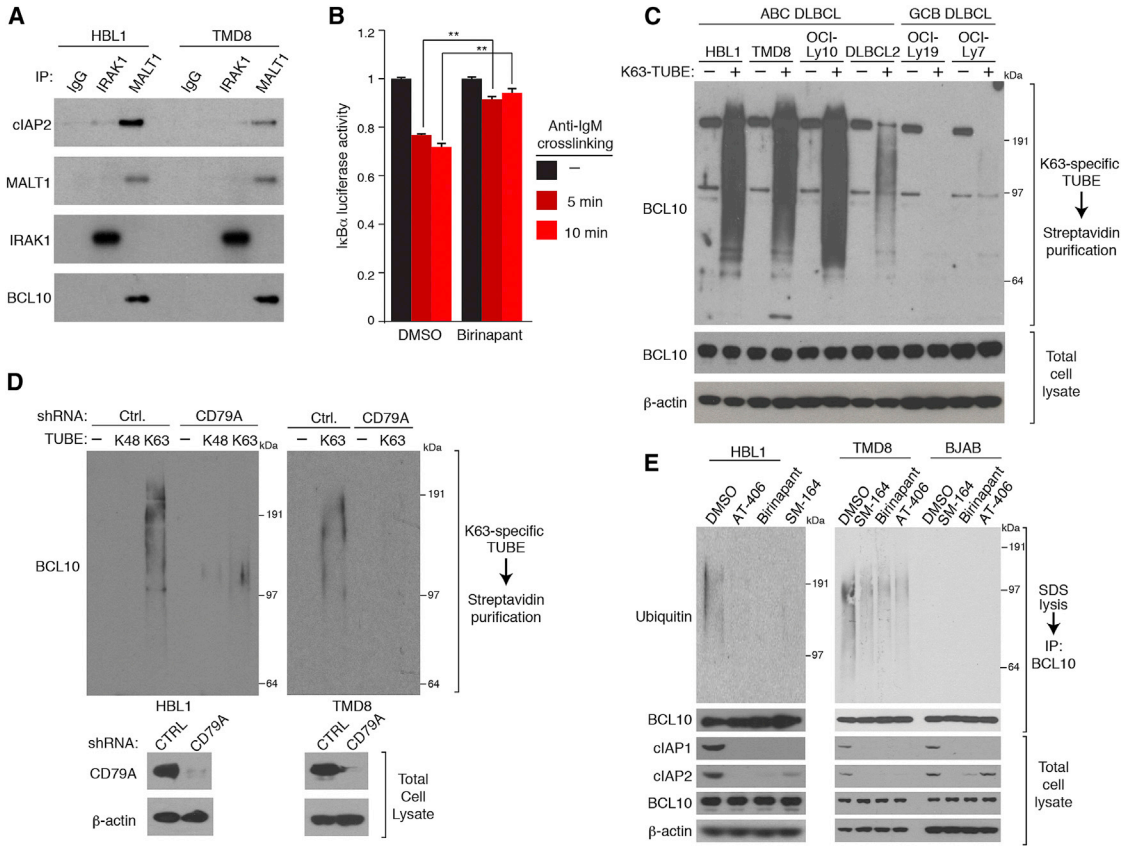

Figure 3. cIAP1/2 Participate in Chronic Active BCR Signaling in ABC DLBCL

(A) Immunoprecipitates (IPs) from ABC DLBCL lines using the indicated antibodies were immunoblotted for the indicated proteins.

(B) Relative luciferase activity of an IκBα-luciferase fusion protein in TMD8 cells treated with birinapant (5 μM) for 6 hr and then with an anti-IgM antibody (10 μg/ml) for the indicated times. Reporter activity was normalized to values from DMSO-treated samples at time 0. Error bars denote SEM of triplicates. p Values (Student's t test) compare treatment groups with the DMSO control. **$p < 0.01$.

(C) SDS lysates of the indicated lines were subjected to biotin-labeled K63-specific TUBE binding and streptavidin purification. TUBE-purified proteins or total lysates were analyzed by immunoblotting.

(D) ABC DLBCL lines were induced to express a CD79A or control (Ctrl.) shRNA. SDS lysates were mixed with biotin-labeled, K63-specific, or K48-specific TUBEs followed by streptavidin purification. TUBE-purified proteins or total lysates were analyzed by immunoblotting.

(E) SDS (1%) lysates prepared from DLBCL lines treated with the indicated SMAC mimetics (5 μM) for 24 hr, diluted, and subjected to anti-BCL10 immunoprecipitation. IPs or total lysates were analyzed by immunoblotting.

See also Figure S3.

We next used the CRISPR gene-targeting system (Cong et al., 2013; Mali et al., 2013) to probe the function of cIAP1 and cIAP2 genetically. Small guide RNAs (sgRNAs) targeting the cIAP1 and cIAP2 coding regions were coexpressed in HBL1 ABC DLBCL cells with the endonuclease Cas9, as described by Wang et al. (2014). cIAP1 and cIAP2 sgRNAs effectively reduced or eliminated expression of their targets after 16 days, while a control sgRNA had no effect (Figure 2F). Inactivation of cIAP1 or cIAP2 decreased phosphorylation of IKKβ and stabilized the IKK substrate IκBα, indicating lower activity of the classical NF-κB pathway (Figure 2F). Similarly, knockdown of cIAP1 or cIAP2 using small hairpin RNAs (shRNAs) was toxic for BCR-dependent ABC DLBCL lines but not for the BCR-independent OCI-Ly3 line (Figures 2G and S2C). Depletion of both ubiquitin ligases was more toxic than depletion of either alone, indicating that they function in a partially redundant fashion. The gene signatures that were downregulated upon knockdown of cIAP1 and cIAP2 overlapped with those altered by birinapant, many of which reflect NF-κB signaling (Table S2, Figure S2D). Together, these genetic data indicate that cIAP1/2 participate in NF-κB activation in ABC DLBCL.

cIAP1/2 Contribute to Chronic Active BCR Signaling in ABC DLBCL

We next investigated the role of cIAP1/2 in the BCR and MYD88 pathways, both of which govern NF-κB activity in ABC DLBCL. cIAP2 co-immunoprecipitated with the MALT1 subunit of the CBM complex in two ABC DLBCL lines, suggesting a role for cIAP2 in BCR signaling (Figure 3A). By contrast, little if any association between cIAP2 and IRAK1, which mediates MYD88 signaling in these ABC DLBCL lines, was detected. To test whether cIAP1/2 contribute to BCR-dependent IKK activity, we engineered TMD8 cells to express an IKK reporter consisting of the IKK substrate IκBα fused to luciferase

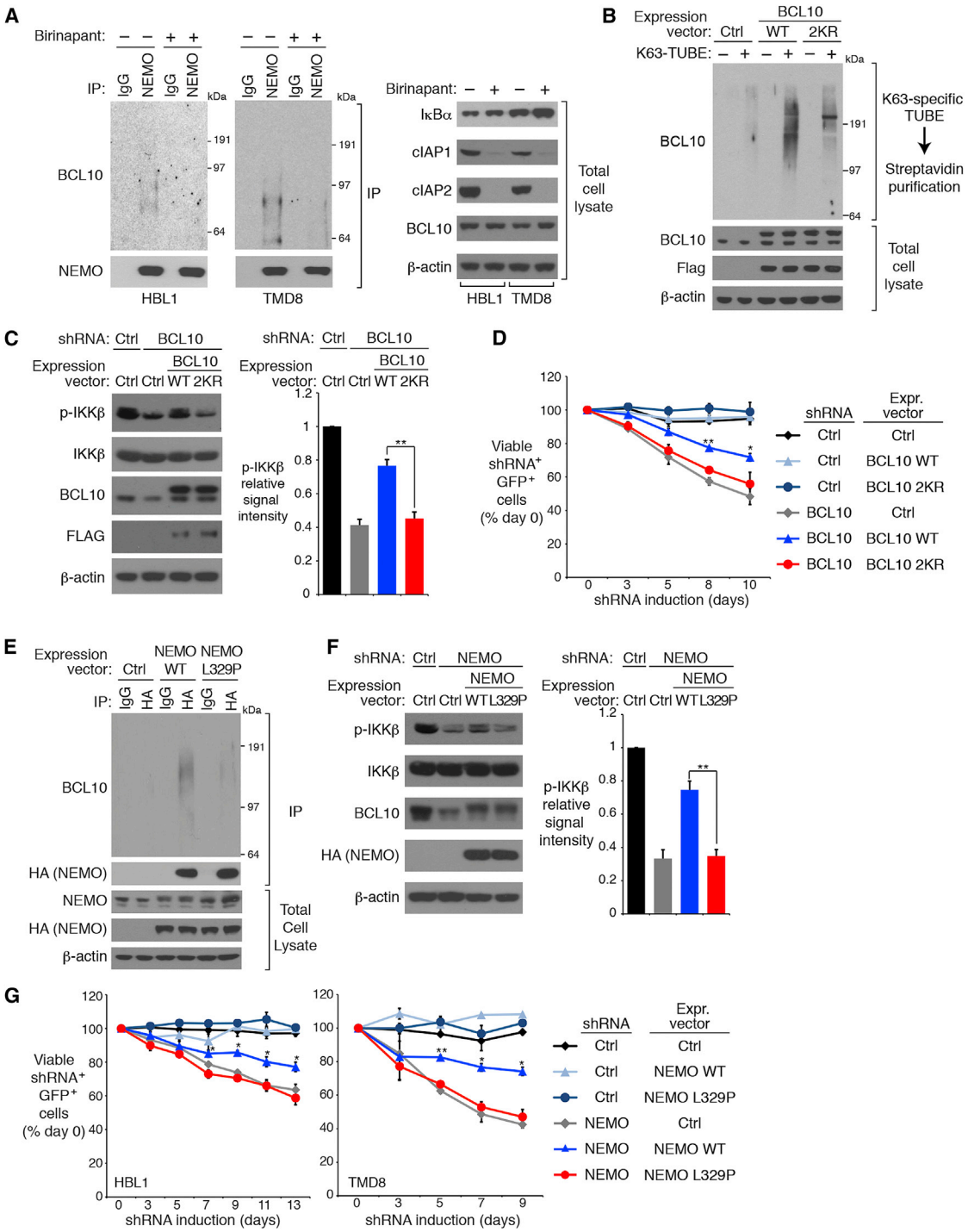

Figure 4. cIAP1/2 Is Required for BCL10 Binding to IKK NEMO in ABC DLBCL

(A) NEMO IPs or total lysates from HBL1 and TMD8 cells treated with birinapant (5 μM) for 24 hr were immunoblotted for the indicated proteins.

(B) Cell lysates of HBL1 cells expressing WT or 2KR mutant BCL10 were subjected to biotin-labeled K63-specific TUBE binding and streptavidin purification, and analyzed by immunoblotting.

(C) Control or BCL10 shRNAs were inducibly expressed in HBL1 cells that had been transduced with WT or 2KR BCL10, or with a control vector. Lysates were analyzed by immunoblotting for the indicated proteins. Relative phospho- (p-) IKKβ levels were quantified by densitometry (right). Error bars denote SEM. p Values (Student's t test) compare the BCL10 WT and 2KR rescue groups.

(D) HBL1 cells transduced with WT or 2KR BCL10, or with a control vector, were induced to express control or BCL10 shRNAs along with GFP. The fraction of viable, $GFP^+/shRNA^+$ cells relative to the live-cell fraction, is plotted at the indicated times following shRNA induction, normalized to day-0 values. Error bars denote SEM. p Values (Student's t test) compare the BCL10 WT and 2KR rescue groups at the indicated time points.

(legend continued on next page)

(Lam et al., 2005). Anti-immunoglobulin M (IgM)-mediated crosslinking of the BCR on the surface of these cells decreased IκBα-luciferase levels within 5–10 min, indicating an increase in IKK activity, but birinapant treatment prevented this IKK activation (Figure 3B). Thus, cIAP1/2 are integral components of the CBM complex that are required for optimal BCR-dependent IKK activation.

Many components of the CBM complex, including TRAF6, MALT1, and BCL10, have been suggested to undergo K63-specific ubiquitination in normal T lymphocytes upon TCR stimulation (Oeckinghaus et al., 2007; Sun et al., 2004; Wu and Ashwell, 2008), but the ubiquitination of these proteins has not been carefully evaluated in DLBCL lines. To address this issue we used biotin-labeled, K63-specific tandem ubiquitin-binding entities (K63-TUBE), which can selectively enrich for polyubiquitinated proteins that have K63 linkages rather than K48 linkages (Silva et al., 2015). K63-TUBE-mediated pulldown in ABC DLBCL lines enriched for ubiquitinated BCL10, which ran as a broad smear in immunoblots, but this was not observed in GCB DLBCL lines (Figure 3C). Inhibition of chronic active BCR signaling by knockdown of the BCR subunit CD79A substantially reduced the levels of K63-ubiquitinated BCL10 in ABC DLBCL lines (Figure 3D). Likewise, SMAC mimetic-mediated depletion of cIAP1 or cIAP2 decreased ubiquitinated BCL10 in BCR-dependent ABC DLBCL lines but not in GCB DLBCL lines (Figure 3E). Depletion of cIAP1/2 had no effect on BCL10 polyubiquitination in OCI-Ly3 cells, which has an activating *CARD11* mutation (Figure S3A), which fits with previous evidence that activating CARD11 mutants can induce BCL10 ubiquitination (Chan et al., 2013). Indeed, ectopic expression of a constitutively active CARD11 mutant in ABC DLBCL cells with a wild-type (WT) *CARD11* locus counteracted birinapant toxicity, leading to selective outgrowth of these transduced cells (Figure S3B).

In contrast to the pronounced K63 ubiquitination of BCL10 in ABC DLBCL lines, little if any K48 ubiquitination of BCL10 could be detected using a K48-specific TUBE (Figure 3D), and BCL10 protein stability was unchanged following depletion of cIAP1/2 with birinapant (Figure S3C). Thus, cIAP1/2 act downstream of BCR signaling to modify BCL10 with K63-linked polyubiquitin in ABC DLBCL.

cIAP1/2-Dependent BCL10 Ubiquitination Promotes IKK Recruitment to the CBM Complex

Following TCR signaling, K63 polyubiquitination of BCL10 is recognized by the UBAN ubiquitin-binding domain of the IKK NEMO subunit, resulting in the recruitment of IKK to the CBM complex (Wu and Ashwell, 2008). In ABC DLBCL cell lines, ubiquitinated BCL10 constitutively associated with NEMO, which was abrogated by treatment with SMAC mimetics (Figures 4A and S4A). Likewise, the constitutive binding of NEMO to MALT1, another component in CBM complex, was also inhibited by birinapant treatment of ABC DLBCL lines (Figure S4B). Thus, K63 polyubiquitination by cIAP1/2 is essential for IKK recruitment to the CBM complex in ABC DLBCL.

Of the 15 lysine residues in BCL10, K31 and K63 are apparent attachment sites for K63 polyubiquitin in TCR signaling (Wu and Ashwell, 2008). To probe the function of BCL10 ubiquitination in ABC DLBCL cells, we ectopically expressed WT BCL10 or the BCL10 2KR mutant in which both K31 and K63 were changed to arginine. BCL10, enriched using the K63-specific TUBE from cells transduced with WT BCL10, ran as a polyubiquitinated protein smear, which was significantly reduced in cells expressing BCL10 2KR (Figure 4B). To assess the contribution of BCL10 ubiquitination to NF-κB activity and viability in ABC DLBCL, we knocked down endogenous BCL10 using an shRNA targeting the BCL10 3′ UTR and ectopically expressed WT or 2KR BCL10 coding regions. BCL10 knockdown decreased IKKβ phosphorylation, which was restored by WT but not 2KR BCL10 (Figure 4C). Similarly, the toxicity of BCL10 knockdown in ABC DLBCL cells was reversed by ectopic provision of WT but not 2KR BCL10 (Figure 4D).

To further assess the impact of BCL10 polyubiquitination on NF-κB activation in ABC DLBCL, we engineered HBL1 cells to express either WT IKK NEMO or the L329P mutant that abrogates ubiquitin binding by the NEMO UBAN domain (Wu et al., 2006). Polyubiquitinated BCL10 was co-immunoprecipitated with WT NEMO but not with the L329P mutant (Figure 4E). NF-κB pathway activity, as judged by IKKβ phosphorylation, was decreased by NEMO knockdown, which could be reversed by ectopic expression of WT but not L329P NEMO (Figure 4F). Likewise, the toxicity of NEMO knockdown for ABC DLBCL lines was mitigated by re-expression of WT but not L329P NEMO (Figure 4G). Overall, our data support a model in which cIAP1/2-dependent polyubiquitination of BCL10 promotes IKK recruitment to the CBM complex in a fashion that depends on ubiquitin binding by IKK NEMO.

LUBAC Recruitment to the CBM Complex in ABC DLBCL Depends on cIAP1/2

In ABC DLBCL lines with chronic active BCR signaling, LUBAC associates constitutively with the CBM complex, where it recognizes and linearly ubiquitinates IKK NEMO (Yang et al., 2014). The LUBAC subunit SHARPIN associated with the CBM component MALT1 in BCR-dependent ABC DLBCL lines but not in GCB DLBCL lines, but treatment with SMAC mimetics reduced this association (Figures 5A and S5A). The zinc-finger domain of the LUBAC subunit RNF31 binds preferentially to K63-polyubiquitin chains, which is essential for

(E) Anti-HA IPs or total lysates of HBL1 cells expressing the indicated HA epitope-tagged WT or L329P mutant NEMO were analyzed by immunoblotting for the indicated proteins.

(F) Control or NEMO shRNAs were inducibly expressed in HBL1 cells that had been transduced with WT or L329P NEMO, or with an empty vector. Lysates were analyzed by immunoblotting for the indicated proteins. Relative p-IKKβ levels were quantified by densitometry. Error bars denote SEM. p Values (Student's t test) compare the NEMO WT and L329P rescue groups.

(G) Cells transduced with WT or L329P NEMO, or with a control vector, were induced to express control or NEMO shRNAs along with GFP. The fraction of viable, $GFP^+/shRNA^+$ cells relative to the live-cell fraction is plotted at the indicated times following shRNA induction, normalized to day-0 values. Error bars denote SEM. p Values (Student's t test) compare the NEMO WT and L329P rescue groups at the indicated time points.

*$p < 0.05$; **$p < 0.01$. See also Figure S4.

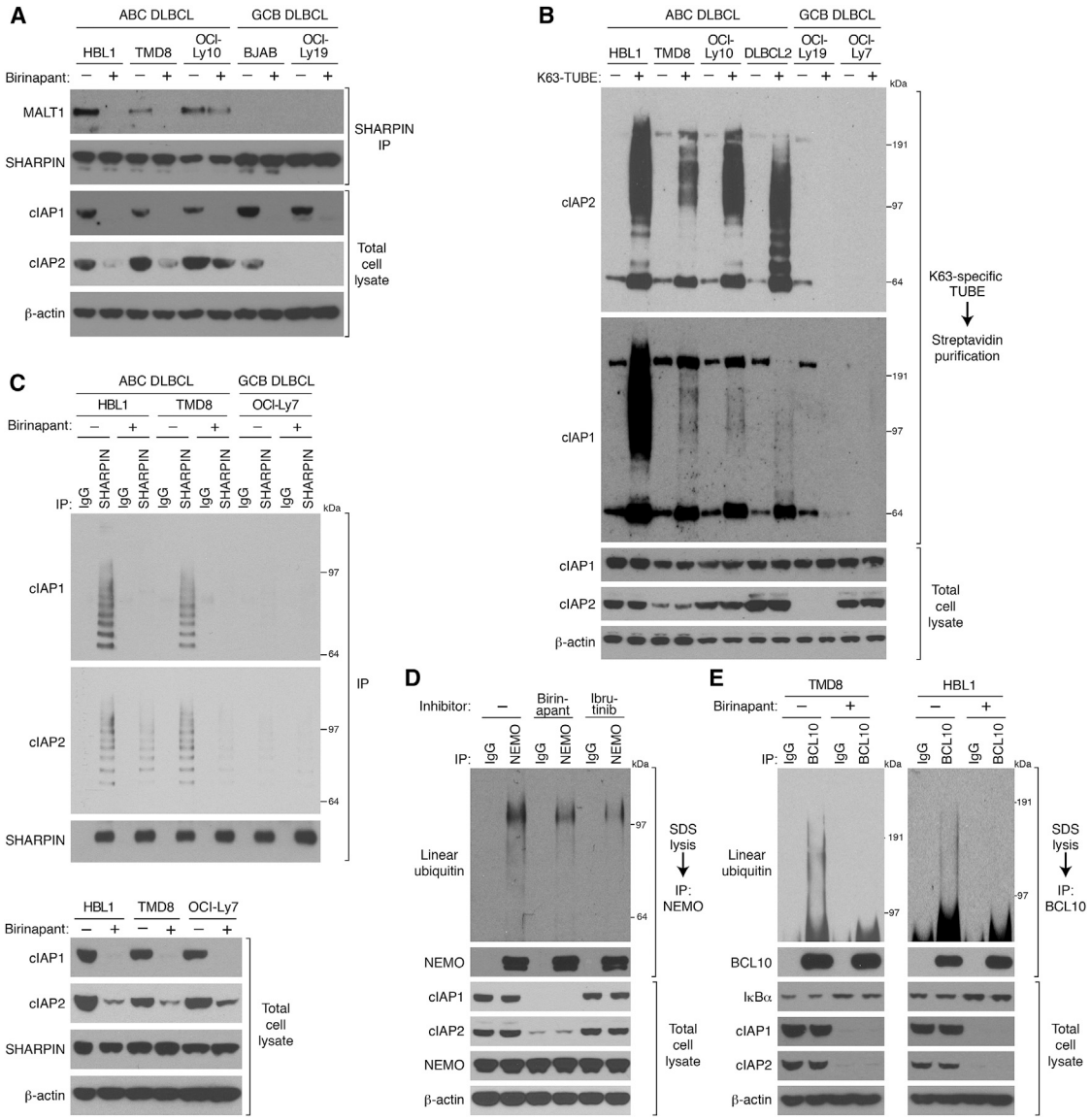

Figure 5. LUBAC Recruitment to the CBM Complex in ABC DLBCL Depends on cIAP1/2

(A) SHARPIN IPs or total lysates of the indicated DLBCL lines treated with birinapant (5 μM) for 24 hr were immunoblotted for the indicated proteins.

(B) Total SDS lysates after biotin-labeled K63-specific TUBE binding and streptavidin purification from the indicated DLBCL lines were analyzed by immunoblotting.

(C) SHARPIN IPs of DLBCL lines treated with birinapant (5 μM) for 24 hr or total lysates were immunoblotted for the indicated proteins.

(D) Lysates prepared using 1% SDS from HBL1 cells treated with birinapant (5 μM) or ibrutinib (10 nM) for 24 hr were diluted and then subjected to immunoprecipitation. IPs or total lysates were immunoblotted for the indicated proteins.

(E) Lysates prepared using 1% SDS from ABC DLBCL cells treated with birinapant (5 μM) for 24 hr were diluted and subjected to immunoprecipitation. IPs or total lysates were immunoblotted for the indicated proteins.

See also Figure S5.

LUBAC recruitment to receptor complexes (Gerlach et al., 2011; Haas et al., 2009; Ikeda et al., 2011). The SHARPIN-MALT1 association was equivalent in cells expressing either WT or 2KR BCL10, suggesting that BCL10 ubiquitination by cIAP1/2 is not necessary for LUBAC recruitment (Figure S5B). We therefore tested whether LUBAC might directly interact with K63-polyubiquitin chains formed on cIAP1/2 by autoubiquitination (Blankenship et al., 2009). Using a K63-specific TUBE assay, we observed abundant K63 polyubiquitination of cIAP1 and cIAP2 in ABC but not GCB DLBCL lines (Figure 5B). By co-immunoprecipitation, SHARPIN associated with ubiquitinated cIAP1 and cIAP2 in two ABC DLBCL lines but not in a GCB DLBCL line, and this association was prevented by SMAC mimetics (Figures 5C and S5C), suggesting that autoubiquitination of cIAP1/2 could be responsible for LUBAC recruitment to the CBM complex.

Given the role of cIAP1/2 in recruiting LUBAC to the CBM complex, we assessed the influence of birinapant on linear ubiquitination of NEMO (Figure 5D). Birinapant partially inhibited linear ubiquitination of NEMO in HBL1 cells, as did treatment with the BTK inhibitor ibrutinib, which inhibits CBM activity. The residual NEMO ubiquitination may be mediated by MYD88, since LUBAC also associates with the mutant MYD88 signaling complex in ABC DLBCL cells (Yang et al., 2014). A recent study revealed that BCL10 is modified by linear polyubiquitin in a mouse B cell line following BCR crosslinking (Satpathy et al., 2015). BCL10 was also linearly ubiquitinated in ABC DLBCL lines, and SMAC mimetics decreased this modification, in keeping with their ability to block LUBAC recruitment (Figures 5E and S5D). Linear ubiquitin chains could either attach to BCL10 directly or contribute to branched polyubiquitin chains that are built upon K63-linked chains attached to BCL10, as described during interleukin-1 signaling (Emmerich et al., 2013). In summary, cIAP1/2-mediated polyubiquitination is required for the recruitment of LUBAC to the CBM complex and the linear ubiquitination of NEMO and BCL10.

Role of cIAP1/2 in Alternative NF-κB Pathway Activation in ABC DLBCL

In normal B cells, cIAP1/2 promote the K48 polyubiquitination and destruction of NIK, a kinase that activates the alternative NF-κB pathway (Vallabhapurapu et al., 2008; Zarnegar et al., 2008a). Consequently, loss of cIAP1/2 leads to NIK stabilization, IKKα activation, proteolytic processing of NFKB2 from its p100 isoform to its p52 isoform, and nuclear accumulation of the alternative NF-κB heterodimer p52/RelB. In untreated ABC DLBCL lines we observed little NIK protein expression, but 6-hr treatment with birinapant caused NIK to accumulate and induced the processing of NFKB2 p100 into p52 (Figure 6A). Treatment of HBL1 cells for 1 day with birinapant decreased nuclear NF-κB binding activity involving the p65 and p50 subunits, consistent with the role of cIAP1/2 in promoting IKKβ activation of the classical NF-κB pathway (Figure 6B). In contrast, birinapant treatment increased NF-κB motif binding by p52 and RelB, consistent with NIK stabilization and activation of the alternative NF-κB pathway (Figure 6B). Treatment with an NIK inhibitor decreased p52 and RelB DNA binding (Figure 6B), suggesting that HBL1 cells have a basal degree of alternative NF-κB activation, a view supported by their low NIK protein levels and basal processing of NFKB2 into the p52 isoform (Figure 6A). Knockdown of NIK, IKKα, or RELB as well as treatment with a NIK inhibitor decreased the NF-κB pathway activity in HBL1 cells (Figures 6C and 6D). Addition of birinapant further decreased NF-κB activity, consistent with combined inhibition of the classical and alternative NF-κB pathways (Figures 6C and 6D). Accordingly, birinapant had more toxicity for HBL1 cells when the alternative NF-κB pathway was simultaneously inhibited by NIK, IKKα, or RELB shRNAs, or by the NIK inhibitor (Figures 6E and 6F).

While treatment with birinapant for 1 day stabilized NIK in two ABC DLBCL lines, NIK levels dropped unexpectedly over the next 2 weeks of treatment, despite addition of fresh birinapant every 3 days (Figure 6G). Interestingly, TRAF3 levels increased during prolonged birinapant treatment, which could contribute to the fall of NIK levels over time (see Discussion) and are consistent with reports of cIAP1/2-mediated K48 polyubiquitination and degradation of TRAF3 (Figure 6G) (Vallabhapurapu et al., 2008; Zarnegar et al., 2008b). Thus, at early time points the decrease in classical NF-κB activity caused by birinapant is counterbalanced by an increase in alternative NF-κB activity, but at later time points birinapant primarily decreases classical NF-κB activity.

Birinapant Is Selectively Toxic for BCR-Dependent ABC DLBCL Models

To investigate the therapeutic potential of SMAC mimetics in DLBCL, we determined the viability of ABC and GCB DLBCL lines after treatment with birinapant for 5 days (Figures 7A and S6A). In all six ABC DLBCL lines with chronic active BCR signaling, birinapant was toxic in a dose-dependent manner. By contrast, birinapant had little if any toxicity for two BCR-independent ABC DLBCL lines or for seven GCB DLBCL lines. Birinapant treatment induced apoptotic cell death in BCR-dependent ABC DLBCL lines, as measured by cleavage of both PARP and caspase 3 (Figure 7B). Two other SMAC mimetics, AT-406 and SM-164, exhibited similar efficacy and specificity in killing BCR-dependent ABC DLBCL lines (Figures S6B and S6C).

We next investigated whether birinapant would combine favorably with other drugs that inhibit oncogenic survival mechanisms in ABC DLBCL. The anti-apoptotic protein BCL2 is highly expressed in ABC DLBCL, and BCL2 inhibition by BH3 mimetics is toxic to ABC DLBCL lines (Mathews Griner et al., 2014). Since birinapant as a single agent induced apoptotic cell death in ABC DLBCL cells (Figure 7B), we combined it with the BH3 mimetic ABT-199 and observed synergistic effects on the viability of three BCR-dependent ABC DLBCL lines (Figure 7C). Since the viability data in these plots were normalized to remove the effect of birinapant as a single agent, the left shift of the toxicity curves indicates more than additive (i.e. synergistic) toxicity of the drug combination, a view further confirmed by a formal mathematical algorithm (Greco et al., 1990) (Figure S6D). By contrast, birinapant did not synergize with the BTK inhibitor ibrutinib, which is understandable since these two drugs target closely related nodes within the BCR pathway (Figure S6E).

Finally, we evaluated the ability of birinapant to retard the growth of ABC DLBCL xenografts. We established ABC DLBCL xenograft mouse models using the HBL1 and DLBCL2 cell lines. In both models, oral treatment with birinapant significantly slowed tumor growth (Figures 7D and S7A) and reduced cIAP1 and cIAP2 protein levels (Figures 7E and S7B). NIK protein levels in HBL1 xenografts after 1 or 2 weeks of treatment were substantially lower than in HBL1 cells treated in vitro with birinapant for 1 day (Figure 7E), in keeping with the drop in NIK protein levels observed after prolonged in vitro treatment with birinapant (Figure 6G). Accordingly, IκBα accumulation and IKKβ phosphorylation reduction were observed in the HBL1 xenografts at the treatment endpoint (Figures 7E and S7C), indicating NF-κB pathway inhibition. At the doses used, birinapant was well tolerated by mice, with no change in body weight or hematologic parameters (Figures S7D–S7F).

DISCUSSION

We describe a role for the E3 ubiquitin ligases cIAP1 and cIAP2 in the oncogenic BCR signaling that characterizes

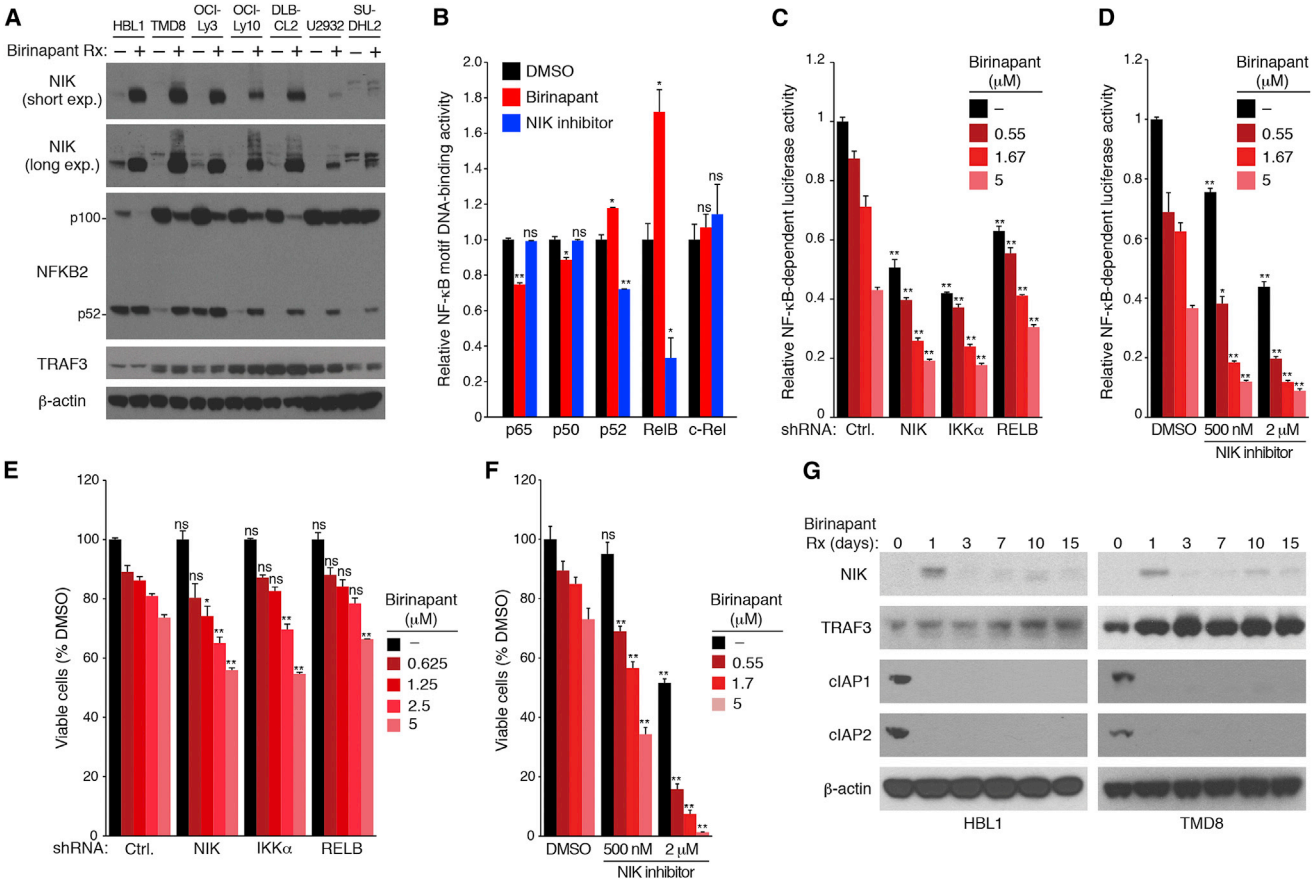

Figure 6. Negative Regulation of Alternative NF-κB Activity by cIAP1/2 in ABC DLBCL

(A) Lysates of ABC DLBCL lines treated with birinapant (5 μM) for 6 hr analyzed by immunoblotting for the indicated proteins.

(B) NF-κB DNA-binding activity utilizing the indicated NF-κB subunits determined in nuclear extracts of HBL1 cells treated with birinapant (5 μM) or a NIK inhibitor (1 μM) for 24 hr, relative to DMSO-treated cells.

(C) Relative activity of an NF-κB-dependent luciferase reporter in HBL1 cells expressing the indicated shRNAs for 2 days followed by birinapant treatment for 24 hr.

(D) Relative activity of an NF-κB-dependent luciferase reporter in HBL1 cells following treatment (24 hr) with the indicated concentrations of birinapant ± an NIK inhibitor.

(E) Relative numbers of viable HBL1 cells that were induced to express the indicated shRNAs for 2 days followed by treatment with the indicated birinapant concentrations for 4 days.

(F) Relative viability of HBL1 cells following treatment (4 days) with the indicated concentrations of birinapant ± an NIK inhibitor.

(G) Lysates of HBL1 or TMD8 cells treated with birinapant (2.5 μM) for the indicated times analyzed by immunoblotting for the indicated proteins.

Error bars denote SEM of triplicates. p Values (Student's t test) compare treatment groups with the DMSO control in (B); the control and experimental shRNA groups at the same birinapant concentrations in (C) and (E); and the DMSO and NIK inhibitor groups at the same birinapant concentrations in (D) and (F). ns, no statistical difference; *$p < 0.05$; **$p < 0.01$.

ABC DLBCL, and provide a strategy to exploit this knowledge therapeutically using SMAC mimetics. Based on our functional and biochemical analysis of cIAP1/2 action in ABC DLBCL, we propose a working model for CBM-dependent NF-κB activation involving these ubiquitin ligases (Figure 8). cIAP1/2 reside in the CBM complex in ABC DLBCL and are heavily modified by K63-polyubiquitin chains, presumably due to autoubiquitination. cIAP1/2 recruit the LUBAC ubiquitin ligase to the CBM complex, presumably because K63-polyubiquitin chains are recognized by the NZF1 ubiquitin-binding domain of the LUBAC RNF31 subunit (Fujita et al., 2014; Gerlach et al., 2011; Ikeda et al., 2011). Separately, cIAP1/2 are necessary for IKK recruitment to the CBM complex in a fashion that depends on BCL10 ubiquitination. BCL10 is modified by both K63-polyubiquitin and linear polyubiquitination in ABC DLBCL, and both modifications depend on cIAP1/2. The recruitment of IKK NEMO depends on its UBAN ubiquitin-binding domain, which binds both K63 and linear polyubiquitin chains with different relative affinities (Kensche et al., 2012; Ngadjeua et al., 2013). Conceivably, the initial recruitment of IKK to the CBM complex may depend on its interaction with K63-ubiquitinated BCL10, while IKK retention in the CBM complex may be fostered by linear ubiquitination of BCL10 subsequent to LUBAC recruitment to the CBM complex. As a consequence of these several biochemical activities, cIAP1/2 contribute significantly to BCR-dependent activation of NF-κB in ABC

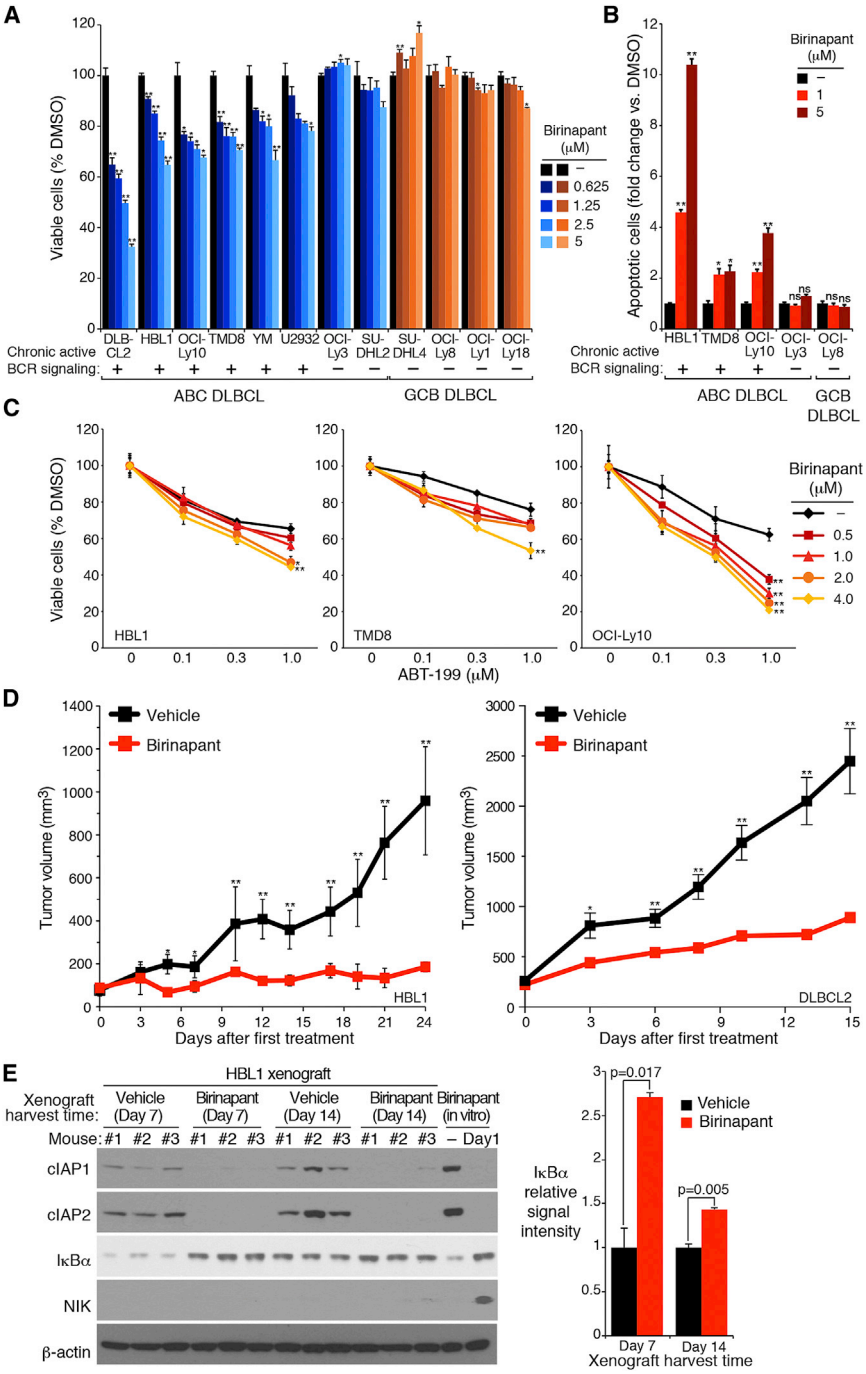

Figure 7. Selective Toxicity of Birinapant for BCR-Dependent ABC DLBCL Lines

(A) Viability of the indicated DLBCL lines treated with birinapant at the indicated concentrations for 5 days, normalized to DMSO-treated cells.

(B) Relative apoptotic cells in DLBCL lines treated with birinapant (2 days) at the indicated concentrations, normalized to DMSO-treated cells.

(C) Viability of ABC DLBCL lines after treatment (4 days) with the indicated concentrations of birinapant, ABT-199, or both. Data are normalized to DMSO-treated cells and then to cells treated with birinapant alone.

(D) NOD/SCID mice bearing HBL1 (left) and DLBCL2 (right) xenografts were treated with birinapant or vehicle. Tumor growth was measured as a function of tumor volume. Error bars denote SEM of n = 3 (HBL1) or n = 5 (DLBCL2).

(E) HBL1 cells were established and treated as in (D). Cell lysates from malignant cells purified from tumors were immunoblotted for the indicated protein. Relative IκBα levels were quantified by densitometry (right).

Error bars denote SEM of triplicates. P values (Student's t test) compare the vehicle and birinapant groups in (A), (B), and (E), or the ABT-199-only group with the birinapant plus ABT-199 group at the highest ABT-199 concentration (C). *p < 0.05; **p < 0.01. See also Figures S6 and S7.

native NF-κB activation (Bea et al., 2013; Puente et al., 2015; Rahal et al., 2014; Rossi et al., 2012). Inactivating mutations of *BIRC3* have not been reported in genomic analyses of DLBCL (Lohr et al., 2012; Morin et al., 2011; Pasqualucci et al., 2011; Zhang et al., 2013), which is consistent with our evidence that cIAP2 is required for BCR-dependent NF-κB activation in ABC DLBCL. In CLL and MCL cases with *BIRC3* mutations the *BIRC2* locus is invariably unmutated, raising the possibility that cIAP1 could maintain BCR signaling in these cases.

During prolonged birinapant treatment over several days, NIK levels dropped and alternative NF-κB activity waned, suggesting that a negative feedback loop was triggered. During this extended time course TRAF3 protein levels rose, in keeping with previous studies showing that cIAP1/2 mediate the degradation of TRAF3 (Vallabhapurapu et al., 2008; Zarnegar et al., 2008b). The rise in TRAF3 could conceivably be responsible for the fall in NIK levels, since birinapant-treated cells have residual cIAP1/2 that could work with TRAF3 and TRAF2 to degrade NIK.

Previous studies of SMAC mimetics in cancer have emphasized their ability to sensitize cancer cells to pro-apoptotic stimuli and to switch the response of cancer cells to TNF-α from survival to death (Fulda and Vucic, 2012). By contrast, SMAC mimetics target chronic active BCR signaling in ABC DLBCL by eliminating DLBCL, accounting for the selective toxicity of SMAC mimetics in BCR-dependent ABC DLBCL lines.

Copy number analysis of DLBCL tumors revealed gain or amplification of the *BIRC2*/*BIRC3* locus in ~16% of ABC but not GCB DLBCL tumors, providing genetic evidence to support an essential role for cIAP1/2 in chronic active BCR signaling in ABC DLBCL. Interestingly, inactivating mutations in *BIRC3* are recurrent in chronic lymphocytic leukemia (CLL; ~9% of cases), mantle cell lymphoma (MCL; ~6%–10% of cases), and splenic marginal zone lymphoma (~5% of cases), and lead to the alter-

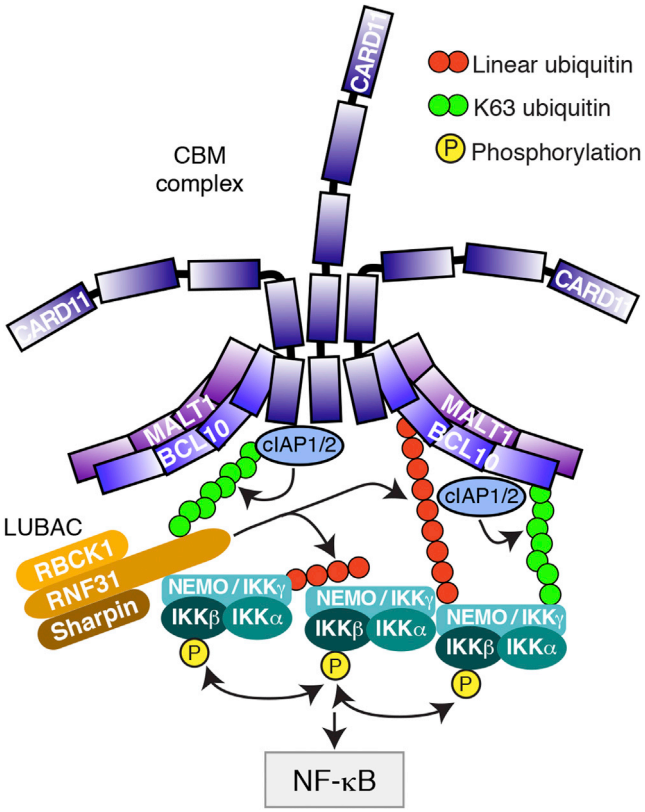

Figure 8. Model of cIAP1/2 Action in the CBM Complex
The cartoon depicts a working model of how cIAP1/2 K63 ubiquitination controls the recruitment of LUBAC and IKK to the CBM complex, thereby activating IKK activation and increasing NF-κB levels in ABC DLBCL.

cIAP1/2, which we have shown are intrinsic components of the CBM complex that are necessary for BCR-dependent NF-κB activation. From this perspective, SMAC mimetics could be more effective against ABC DLBCL than against solid tumors because they directly target an essential oncogenic pathway in ABC DLBCL. Based on our mechanistic and functional studies, clinical evaluation of SMAC mimetics in DLBCL should proceed selectively in the ABC DLBCL subtype, both as a single agent and in combination with other drugs that inhibit pro-survival pathways in ABC DLBCL, such as the BCL2 inhibitor ABT-199.

EXPERIMENTAL PROCEDURES

See Supplemental Experimental Procedures for full details.

Patient Samples

All samples were studied according to a protocol approved by the National Cancer Institute Institutional Review Board.

BIRC2 and *BIRC3* Copy Number Analysis

Affymetrix 250k-Sty SNP array data were downloaded from the GEO database (http://www.ncbi.nlm.nih.gov/geo/) using accession number GEO: GSE57612. Gains and losses were determined by the GLAD method, implemented in R. Affymetrix SNP 6.0 data were analyzed using the Aroma algorithm, and segments assigned to copy categories as described by Lenz et al. (2008b). Differences in *BIRC2*/*BIRC3* copy number prevalence between ABC and GCB DLBCL was tested using Fisher's exact test.

Cell Culture

Cell lines for inducible shRNA-mediated knockdown were modified to express an ecotropic retroviral receptor and a fusion protein of the Tet repressor and the blasticidin resistance gene, as described previously (Ngo et al., 2006). For CRISPR-Cas9 knockdown, cells were transduced with lentiviruses expressing Cas9 and an sgRNA (lentiCRISPR), as described by Shalem et al. (2014).

Tumor Model and Therapy Study

Animal experiments were approved by the National Cancer Institute Animal Care and Use Committee (NCI ACUC) and were performed in accordance with NCI ACUC guidelines. Human ABC DLBCL xenograft models were established by subcutaneous injection of lymphoma cell lines into NOD/SCID (non-obese diabetic/severe combined immunodeficient) mice. For biochemical analysis, xenografts were harvested 24 hr after final dosing with birinapant or vehicle, and lymphoma cells were purified from mouse cells using the MACS Mouse Cell Depletion Kit (Miltenyi Biotec).

ACCESSION NUMBERS

Genomic data has been submitted to the GEO database (http://www.ncbi.nlm.nih.gov/geo/) with the accession numbers GEO: GSE73281 and GSE73639.

SUPPLEMENTAL INFORMATION

Supplemental Information includes Supplemental Experimental Procedures, seven figures, and two tables and can be found with this article online at http://dx.doi.org/10.1016/j.ccell.2016.03.006.

AUTHOR CONTRIBUTIONS

Y.Y. and L.M.S. designed and oversaw the project. Y.Y., P.K., A.L.S., R.S., and R.M.Y. performed experiments and collected data. Y.Y., P.K., A.L.S., and L.M.R. analyzed and interpreted the data. A.L.S. analyzed Affymetrix microarray data. X.L., D.W.H., D.W., and G.W.W. analyzed aCGH and Affymetrix SNP6.0 data. H.M.Y., M.N., M.C., Y.Y., H.Z., X.Y., and W.X. provided technical support and critical materials. W.C.C., E.S.J., R.D.G., E.C., A.R., G.O., J.D., and L.R. provided tumor samples. Y.Y. and L.M.S. wrote the manuscript.

ACKNOWLEDGMENTS

The authors thank the patients for their participation. We wish to thank Kathleen Meyer for her assistance with GEO submissions, and the members of the Coriell Genotyping and Microarray Center for their assistance with Affymetrix SNP6.0 array. This study was conducted under the auspices of the Lymphoma/Leukemia Molecular Profiling Project (LLMPP). This research was supported by the Intramural Research Program of the NIH, National Cancer Institute, Center for Cancer Research. R.S. was supported by the Dr. Mildred Scheel Stiftung für Krebsforschung (Deutsche Krebshilfe). D.W. is the Philip O'Bryan Montgomery, Jr., MD, Fellow of the Damon Runyon Cancer Research Foundation (DRG-2208-14).

Received: September 22, 2015
Revised: January 27, 2016
Accepted: March 11, 2016
Published: April 11, 2016

REFERENCES

Alizadeh, A.A., Eisen, M.B., Davis, R.E., Ma, C., Lossos, I.S., Rosenwald, A., Boldrick, J.C., Sabet, H., Tran, T., Yu, X., et al. (2000). Distinct types of diffuse large B-cell lymphoma identified by gene expression profiling. Nature *403*, 503–511.

Allensworth, J.L., Sauer, S.J., Lyerly, H.K., Morse, M.A., and Devi, G.R. (2013). Smac mimetic Birinapant induces apoptosis and enhances TRAIL potency in inflammatory breast cancer cells in an IAP-dependent and TNF-alpha-independent mechanism. Breast Cancer Res. Treat. *137*, 359–371.

Annunziata, C.M., Davis, R.E., Demchenko, Y., Bellamy, W., Gabrea, A., Zhan, F., Lenz, G., Hanamura, I., Wright, G., Xiao, W., et al. (2007). Frequent engagement of the classical and alternative NF-kappaB pathways by diverse genetic abnormalities in multiple myeloma. Cancer Cell *12*, 115–130.

Bea, S., Valdes-Mas, R., Navarro, A., Salaverria, I., Martin-Garcia, D., Jares, P., Gine, E., Pinyol, M., Royo, C., Nadeu, F., et al. (2013). Landscape of somatic mutations and clonal evolution in mantle cell lymphoma. Proc. Natl. Acad. Sci. USA *110*, 18250–18255.

Benetatos, C.A., Mitsuuchi, Y., Burns, J.M., Neiman, E.M., Condon, S.M., Yu, G., Seipel, M.E., Kapoor, G.S., Laporte, M.G., Rippin, S.R., et al. (2014). Birinapant (TL32711), a bivalent SMAC mimetic, targets TRAF2-associated cIAPs, abrogates TNF-induced NF-kappaB activation, and is active in patient-derived xenograft models. Mol. Cancer Ther. *13*, 867–879.

Bertrand, M.J., Milutinovic, S., Dickson, K.M., Ho, W.C., Boudreault, A., Durkin, J., Gillard, J.W., Jaquith, J.B., Morris, S.J., and Barker, P.A. (2008). cIAP1 and cIAP2 facilitate cancer cell survival by functioning as E3 ligases that promote RIP1 ubiquitination. Mol. Cell *30*, 689–700.

Blankenship, J.W., Varfolomeev, E., Goncharov, T., Fedorova, A.V., Kirkpatrick, D.S., Izrael-Tomasevic, A., Phu, L., Arnott, D., Aghajan, M., Zobel, K., et al. (2009). Ubiquitin binding modulates IAP antagonist-stimulated proteasomal degradation of c-IAP1 and c-IAP2(1). Biochem. J. *417*, 149–160.

Chan, W., Schaffer, T.B., and Pomerantz, J.L. (2013). A quantitative signaling screen identifies CARD11 mutations in the CARD and LATCH domains that induce Bcl10 ubiquitination and human lymphoma cell survival. Mol. Cell Biol. *33*, 429–443.

Chen, Z.J. (2012). Ubiquitination in signaling to and activation of IKK. Immunol. Rev. *246*, 95–106.

Chu, Z.L., McKinsey, T.A., Liu, L., Gentry, J.J., Malim, M.H., and Ballard, D.W. (1997). Suppression of tumor necrosis factor-induced cell death by inhibitor of apoptosis c-IAP2 is under NF-kappaB control. Proc. Natl. Acad. Sci. USA *94*, 10057–10062.

Condon, S.M., Mitsuuchi, Y., Deng, Y., LaPorte, M.G., Rippin, S.R., Haimowitz, T., Alexander, M.D., Kumar, P.T., Hendi, M.S., Lee, Y.H., et al. (2014). Birinapant, a smac-mimetic with improved tolerability for the treatment of solid tumors and hematological malignancies. J. Med. Chem. *57*, 3666–3677.

Cong, L., Ran, F.A., Cox, D., Lin, S., Barretto, R., Habib, N., Hsu, P.D., Wu, X., Jiang, W., Marraffini, L.A., and Zhang, F. (2013). Multiplex genome engineering using CRISPR/Cas systems. Science *339*, 819–823.

Davis, R.E., Brown, K.D., Siebenlist, U., and Staudt, L.M. (2001). Constitutive nuclear factor kappa B activity is required for survival of activated B Cell-like diffuse large B cell lymphoma cells. J. Exp. Med. *194*, 1861–1874.

Davis, R.E., Ngo, V.N., Lenz, G., Tolar, P., Young, R.M., Romesser, P.B., Kohlhammer, H., Lamy, L., Zhao, H., Yang, Y., et al. (2010). Chronic active B-cell-receptor signalling in diffuse large B-cell lymphoma. Nature *463*, 88–92.

Dueber, E.C., Schoeffler, A.J., Lingel, A., Elliott, J.M., Fedorova, A.V., Giannetti, A.M., Zobel, K., Maurer, B., Varfolomeev, E., Wu, P., et al. (2011). Antagonists induce a conformational change in cIAP1 that promotes autoubiquitination. Science *334*, 376–380.

Eckelman, B.P., and Salvesen, G.S. (2006). The human anti-apoptotic proteins cIAP1 and cIAP2 bind but do not inhibit caspases. J. Biol. Chem. *281*, 3254–3260.

Emmerich, C.H., Ordureau, A., Strickson, S., Arthur, J.S., Pedrioli, P.G., Komander, D., and Cohen, P. (2013). Activation of the canonical IKK complex by K63/M1-linked hybrid ubiquitin chains. Proc. Natl. Acad. Sci. USA *110*, 15247–15252.

Fujita, H., Rahighi, S., Akita, M., Kato, R., Sasaki, Y., Wakatsuki, S., and Iwai, K. (2014). Mechanism underlying IkappaB kinase activation mediated by the linear ubiquitin chain assembly complex. Mol. Cell Biol. *34*, 1322–1335.

Fulda, S., and Vucic, D. (2012). Targeting IAP proteins for therapeutic intervention in cancer. Nat. Rev. Drug Discov. *11*, 109–124.

Gardam, S., Turner, V.M., Anderton, H., Limaye, S., Basten, A., Koentgen, F., Vaux, D.L., Silke, J., and Brink, R. (2011). Deletion of cIAP1 and cIAP2 in murine B lymphocytes constitutively activates cell survival pathways and inactivates the germinal center response. Blood *117*, 4041–4051.

Gerlach, B., Cordier, S.M., Schmukle, A.C., Emmerich, C.H., Rieser, E., Haas, T.L., Webb, A.I., Rickard, J.A., Anderton, H., Wong, W.W., et al. (2011). Linear ubiquitination prevents inflammation and regulates immune signalling. Nature *471*, 591–596.

Greco, W.R., Park, H.S., and Rustum, Y.M. (1990). Application of a new approach for the quantitation of drug synergism to the combination of cis-diamminedichloroplatinum and 1-beta-D-arabinofuranosylcytosine. Cancer Res. *50*, 5318–5327.

Haas, T.L., Emmerich, C.H., Gerlach, B., Schmukle, A.C., Cordier, S.M., Rieser, E., Feltham, R., Vince, J., Warnken, U., Wenger, T., et al. (2009). Recruitment of the linear ubiquitin chain assembly complex stabilizes the TNF-R1 signaling complex and is required for TNF-mediated gene induction. Mol. Cell *36*, 831–844.

Ikeda, F., Deribe, Y.L., Skanland, S.S., Stieglitz, B., Grabbe, C., Franz-Wachtel, M., van Wijk, S.J., Goswami, P., Nagy, V., Terzic, J., et al. (2011). SHARPIN forms a linear ubiquitin ligase complex regulating NF-kappaB activity and apoptosis. Nature *471*, 637–641.

Keats, J.J., Fonseca, R., Chesi, M., Schop, R., Baker, A., Chng, W.J., Van Wier, S., Tiedemann, R., Shi, C.X., Sebag, M., et al. (2007). Promiscuous mutations activate the noncanonical NF-kappaB pathway in multiple myeloma. Cancer Cell *12*, 131–144.

Kensche, T., Tokunaga, F., Ikeda, F., Goto, E., Iwai, K., and Dikic, I. (2012). Analysis of nuclear factor-kappaB (NF-kappaB) essential modulator (NEMO) binding to linear and lysine-linked ubiquitin chains and its role in the activation of NF-kappaB. J. Biol. Chem. *287*, 23626–23634.

Krepler, C., Chunduru, S.K., Halloran, M.B., He, X., Xiao, M., Vultur, A., Villanueva, J., Mitsuuchi, Y., Neiman, E.M., Benetatos, C., et al. (2013). The novel SMAC mimetic birinapant exhibits potent activity against human melanoma cells. Clin. Cancer Res. *19*, 1784–1794.

Lam, L.T., Davis, R.E., Pierce, J., Hepperle, M., Xu, Y., Hottelet, M., Nong, Y., Wen, D., Adams, J., Dang, L., and Staudt, L.M. (2005). Small molecule inhibitors of IkappaB kinase are selectively toxic for subgroups of diffuse large B-cell lymphoma defined by gene expression profiling. Clin. Cancer Res. *11*, 28–40.

Lenz, G., Davis, R.E., Ngo, V.N., Lam, L., George, T.C., Wright, G.W., Dave, S.S., Zhao, H., Xu, W., Rosenwald, A., et al. (2008a). Oncogenic CARD11 mutations in human diffuse large B cell lymphoma. Science *319*, 1676–1679.

Lenz, G., Wright, G.W., Emre, N.C., Kohlhammer, H., Dave, S.S., Davis, R.E., Carty, S., Lam, L.T., Shaffer, A.L., Xiao, W., et al. (2008b). Molecular subtypes of diffuse large B-cell lymphoma arise by distinct genetic pathways. Proc. Natl. Acad. Sci. USA *105*, 13520–13525.

Liston, P., Roy, N., Tamai, K., Lefebvre, C., Baird, S., Cherton-Horvat, G., Farahani, R., McLean, M., Ikeda, J.E., MacKenzie, A., and Korneluk, R.G. (1996). Suppression of apoptosis in mammalian cells by NAIP and a related family of IAP genes. Nature *379*, 349–353.

Lohr, J.G., Stojanov, P., Lawrence, M.S., Auclair, D., Chapuy, B., Sougnez, C., Cruz-Gordillo, P., Knoechel, B., Asmann, Y.W., Slager, S.L., et al. (2012). Discovery and prioritization of somatic mutations in diffuse large B-cell lymphoma (DLBCL) by whole-exome sequencing. Proc. Natl. Acad. Sci. USA *109*, 3879–3884.

Mali, P., Yang, L., Esvelt, K.M., Aach, J., Guell, M., DiCarlo, J.E., Norville, J.E., and Church, G.M. (2013). RNA-guided human genome engineering via Cas9. Science *339*, 823–826.

Mathews Griner, L.A., Guha, R., Shinn, P., Young, R.M., Keller, J.M., Liu, D., Goldlust, I.S., Yasgar, A., McKnight, C., Boxer, M.B., et al. (2014). High-throughput combinatorial screening identifies drugs that cooperate with ibrutinib to kill activated B-cell-like diffuse large B-cell lymphoma cells. Proc. Natl. Acad. Sci. USA *111*, 2349–2354.

Micheau, O., and Tschopp, J. (2003). Induction of TNF receptor I-mediated apoptosis via two sequential signaling complexes. Cell *114*, 181–190.

Morin, R.D., Mendez-Lago, M., Mungall, A.J., Goya, R., Mungall, K.L., Corbett, R.D., Johnson, N.A., Severson, T.M., Chiu, R., Field, M., et al. (2011). Frequent mutation of histone-modifying genes in non-Hodgkin lymphoma. Nature *476*, 298–303.

Ngadjeua, F., Chiaravalli, J., Traincard, F., Raynal, B., Fontan, E., and Agou, F. (2013). Two-sided ubiquitin binding of NF-kappaB essential modulator (NEMO) zinc finger unveiled by a mutation associated with anhidrotic ectodermal dysplasia with immunodeficiency syndrome. J. Biol. Chem. *288*, 33722–33737.

Ngo, V.N., Davis, R.E., Lamy, L., Yu, X., Zhao, H., Lenz, G., Lam, L.T., Dave, S., Yang, L., Powell, J., and Staudt, L.M. (2006). A loss-of-function RNA interference screen for molecular targets in cancer. Nature *441*, 106–110.

Ngo, V.N., Young, R.M., Schmitz, R., Jhavar, S., Xiao, W., Lim, K.H., Kohlhammer, H., Xu, W., Yang, Y., Zhao, H., et al. (2011). Oncogenically active MYD88 mutations in human lymphoma. Nature *470*, 115–119.

Oeckinghaus, A., Wegener, E., Welteke, V., Ferch, U., Arslan, S.C., Ruland, J., Scheidereit, C., and Krappmann, D. (2007). Malt1 ubiquitination triggers NF-kappaB signaling upon T-cell activation. EMBO J. *26*, 4634–4645.

Park, S.M., Yoon, J.B., and Lee, T.H. (2004). Receptor interacting protein is ubiquitinated by cellular inhibitor of apoptosis proteins (c-IAP1 and c-IAP2) in vitro. FEBS Lett. *566*, 151–156.

Pasqualucci, L., Trifonov, V., Fabbri, G., Ma, J., Rossi, D., Chiarenza, A., Wells, V.A., Grunn, A., Messina, M., Elliot, O., et al. (2011). Analysis of the coding genome of diffuse large B-cell lymphoma. Nat. Genet. *43*, 830–837.

Puente, X.S., Bea, S., Valdes-Mas, R., Villamor, N., Gutierrez-Abril, J., Martin-Subero, J.I., Munar, M., Rubio-Perez, C., Jares, P., Aymerich, M., et al. (2015). Non-coding recurrent mutations in chronic lymphocytic leukaemia. Nature *526*, 519–524.

Rahal, R., Frick, M., Romero, R., Korn, J.M., Kridel, R., Chan, F.C., Meissner, B., Bhang, H.E., Ruddy, D., Kauffmann, A., et al. (2014). Pharmacological and genomic profiling identifies NF-kappaB-targeted treatment strategies for mantle cell lymphoma. Nat. Med. *20*, 87–92.

Rossi, D., Trifonov, V., Fangazio, M., Bruscaggin, A., Rasi, S., Spina, V., Monti, S., Vaisitti, T., Arruga, F., Fama, R., et al. (2012). The coding genome of splenic marginal zone lymphoma: activation of NOTCH2 and other pathways regulating marginal zone development. J. Exp. Med. *209*, 1537–1551.

Rothe, M., Pan, M.G., Henzel, W.J., Ayres, T.M., and Goeddel, D.V. (1995). The TNFR2-TRAF signaling complex contains two novel proteins related to baculoviral inhibitor of apoptosis proteins. Cell *83*, 1243–1252.

Roy, N., Deveraux, Q.L., Takahashi, R., Salvesen, G.S., and Reed, J.C. (1997). The c-IAP-1 and c-IAP-2 proteins are direct inhibitors of specific caspases. EMBO J. *16*, 6914–6925.

Samuel, T., Welsh, K., Lober, T., Togo, S.H., Zapata, J.M., and Reed, J.C. (2006). Distinct BIR domains of cIAP1 mediate binding to and ubiquitination of tumor necrosis factor receptor-associated factor 2 and second mitochondrial activator of caspases. J. Biol. Chem. *281*, 1080–1090.

Satpathy, S., Wagner, S.A., Beli, P., Gupta, R., Kristiansen, T.A., Malinova, D., Francavilla, C., Tolar, P., Bishop, G.A., Hostager, B.S., and Choudhary, C. (2015). Systems-wide analysis of BCR signalosomes and downstream phosphorylation and ubiquitylation. Mol. Syst. Biol. *11*, 810.

Scholtysik, R., Kreuz, M., Hummel, M., Rosolowski, M., Szczepanowski, M., Klapper, W., Loeffler, M., Trumper, L., Siebert, R., Kuppers, R., et al. (2015). Characterization of genomic imbalances in diffuse large B-cell lymphoma by detailed SNP-chip analysis. Int. J. Cancer *136*, 1033–1042.

Shaffer, A.L., Wright, G., Yang, L., Powell, J., Ngo, V., Lamy, L., Lam, L.T., Davis, R.E., and Staudt, L.M. (2006). A library of gene expression signatures to illuminate normal and pathological lymphoid biology. Immunol. Rev. *210*, 67–85.

Shaffer, A.L., 3rd, Young, R.M., and Staudt, L.M. (2012). Pathogenesis of human B cell lymphomas. Annu. Rev. Immunol. *30*, 565–610.

Shalem, O., Sanjana, N.E., Hartenian, E., Shi, X., Scott, D.A., Mikkelsen, T.S., Heckl, D., Ebert, B.L., Root, D.E., Doench, J.G., and Zhang, F. (2014). Genome-scale CRISPR-Cas9 knockout screening in human cells. Science *343*, 84–87.

Shu, H.B., Takeuchi, M., and Goeddel, D.V. (1996). The tumor necrosis factor receptor 2 signal transducers TRAF2 and c-IAP1 are components of the tumor necrosis factor receptor 1 signaling complex. Proc. Natl. Acad. Sci. USA *93*, 13973–13978.

Silva, G.M., Finley, D., and Vogel, C. (2015). K63 polyubiquitination is a new modulator of the oxidative stress response. Nat. Struct. Mol. Biol. *22*, 116–123.

Sun, L., Deng, L., Ea, C.K., Xia, Z.P., and Chen, Z.J. (2004). The TRAF6 ubiquitin ligase and TAK1 kinase mediate IKK activation by BCL10 and MALT1 in T lymphocytes. Mol. Cell *14*, 289–301.

Vallabhapurapu, S., Matsuzawa, A., Zhang, W., Tseng, P.H., Keats, J.J., Wang, H., Vignali, D.A., Bergsagel, P.L., and Karin, M. (2008). Nonredundant and complementary functions of TRAF2 and TRAF3 in a ubiquitination cascade that activates NIK-dependent alternative NF-kappaB signaling. Nat. Immunol. *9*, 1364–1370.

Varfolomeev, E., Blankenship, J.W., Wayson, S.M., Fedorova, A.V., Kayagaki, N., Garg, P., Zobel, K., Dynek, J.N., Elliott, L.O., Wallweber, H.J., et al. (2007). IAP antagonists induce autoubiquitination of c-IAPs, NF-kappaB activation, and TNFalpha-dependent apoptosis. Cell *131*, 669–681.

Varfolomeev, E., Goncharov, T., Fedorova, A.V., Dynek, J.N., Zobel, K., Deshayes, K., Fairbrother, W.J., and Vucic, D. (2008). c-IAP1 and c-IAP2 are critical mediators of tumor necrosis factor alpha (TNFalpha)-induced NF-kappaB activation. J. Biol. Chem. *283*, 24295–24299.

Vince, J.E., Wong, W.W., Khan, N., Feltham, R., Chau, D., Ahmed, A.U., Benetatos, C.A., Chunduru, S.K., Condon, S.M., McKinlay, M., et al. (2007). IAP antagonists target cIAP1 to induce TNFalpha-dependent apoptosis. Cell *131*, 682–693.

Walczak, H., Iwai, K., and Dikic, I. (2012). Generation and physiological roles of linear ubiquitin chains. BMC Biol. *10*, 23.

Wang, C.Y., Mayo, M.W., Korneluk, R.G., Goeddel, D.V., and Baldwin, A.S., Jr. (1998). NF-kappaB antiapoptosis: induction of TRAF1 and TRAF2 and c-IAP1 and c-IAP2 to suppress caspase-8 activation. Science *281*, 1680–1683.

Wang, T., Wei, J.J., Sabatini, D.M., and Lander, E.S. (2014). Genetic screens in human cells using the CRISPR-Cas9 system. Science *343*, 80–84.

Wilson, W.H., Young, R.M., Schmitz, R., Yang, Y., Pittaluga, S., Wright, G., Lih, C.J., Williams, P.M., Shaffer, A.L., Gerecitano, J., et al. (2015). Targeting B cell receptor signaling with ibrutinib in diffuse large B cell lymphoma. Nat. Med. *21*, 922–926.

Wu, C.J., and Ashwell, J.D. (2008). NEMO recognition of ubiquitinated Bcl10 is required for T cell receptor-mediated NF-kappaB activation. Proc. Natl. Acad. Sci. USA *105*, 3023–3028.

Wu, C.J., Conze, D.B., Li, T., Srinivasula, S.M., and Ashwell, J.D. (2006). Sensing of Lys 63-linked polyubiquitination by NEMO is a key event in NF-kappaB activation [corrected]. Nat. Cell Biol. *8*, 398–406.

Yang, Y., Fang, S., Jensen, J.P., Weissman, A.M., and Ashwell, J.D. (2000). Ubiquitin protein ligase activity of IAPs and their degradation in proteasomes in response to apoptotic stimuli. Science *288*, 874–877.

Yang, Y., Schmitz, R., Mitala, J., Whiting, A., Xiao, W., Ceribelli, M., Wright, G.W., Zhao, H., Yang, Y., Xu, W., et al. (2014). Essential role of the linear ubiquitin chain assembly complex in lymphoma revealed by rare germline polymorphisms. Cancer Discov. *4*, 480–493.

Zarnegar, B., Yamazaki, S., He, J.Q., and Cheng, G. (2008a). Control of canonical NF-kappaB activation through the NIK-IKK complex pathway. Proc. Natl. Acad. Sci. USA *105*, 3503–3508.

Zarnegar, B.J., Wang, Y., Mahoney, D.J., Dempsey, P.W., Cheung, H.H., He, J., Shiba, T., Yang, X., Yeh, W.C., Mak, T.W., et al. (2008b). Noncanonical NF-kappaB activation requires coordinated assembly of a regulatory complex of the adaptors cIAP1, cIAP2, TRAF2 and TRAF3 and the kinase NIK. Nat. Immunol. *9*, 1371–1378.

Zhang, J., Grubor, V., Love, C.L., Banerjee, A., Richards, K.L., Mieczkowski, P.A., Dunphy, C., Choi, W., Au, W.Y., Srivastava, G., et al. (2013). Genetic heterogeneity of diffuse large B-cell lymphoma. Proc. Natl. Acad. Sci. USA *110*, 1398–1403.

Zhang, B., Calado, D.P., Wang, Z., Frohler, S., Kochert, K., Qian, Y., Koralov, S.B., Schmidt-Supprian, M., Sasaki, Y., Unitt, C., et al. (2015). An oncogenic role for alternative NF-kappaB signaling in DLBCL revealed upon deregulated BCL6 expression. Cell Rep. *11*, 715–726.

Cancer Cell, Volume *29*

Supplemental Information

Targeting Non-proteolytic Protein Ubiquitination for the Treatment of Diffuse Large B Cell Lymphoma

Yibin Yang, Priscilla Kelly, Arthur L. Shaffer, III, Roland Schmitz, Hee Min Yoo, Xinyue Liu, Da Wei Huang, Daniel Webster, Ryan M. Young, Masao Nakagawa, Michele Ceribelli, George W. Wright, Yandan Yang, Hong Zhao, Xin Yu, Weihong Xu, Wing C. Chan, Elaine S. Jaffe, Randy D. Gascoyne, Elias Campo, Andreas Rosenwald, German Ott, Jan Delabie, Lisa Rimsza, and Louis M. Staudt

Supplemental Data

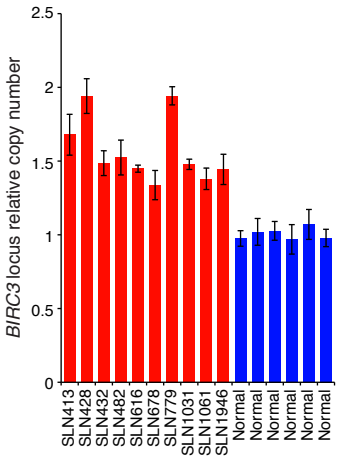

Figure S1, related to Figure 1: Confirmation of *BIRC3* copy number gains by real-time PCR in ABC DLBCL tumors.

Genomic DNA of 10 ABC DLBCL cases and 6 normal controls were isolated, purified and the relative abundance of *BIRC3* copy number were determined by real-time PCR, normalized to a stable control region (*CHMP4A*), and then normalized to the average copy numbers of 6 normal samples. Error bars denote SEM of triplicates.

Table S1, related to Figure 1: Co-occurrence of *BIRC2/BIRC3* copy number gain/amplification with other genetic lesions in ABC DLBCL cases.

Sample Name	*BIRC2/3* copy # status	CARD11 mutational status	CD79A mutational status	CD79B mutational status	MYD88 mutational status	A20 mutational status
ABC DLBCL case #1	Gain/Amp	WT	WT	WT	WT	WT
ABC DLBCL case #2	Gain/Amp	WT	WT	WT	L265P	WT
ABC DLBCL case #3	Gain/Amp	WT	WT	WT	WT	WT
ABC DLBCL case #4	Gain/Amp	WT	WT	Y196C	WT	WT
ABC DLBCL case #5	Gain/Amp	WT	WT	WT	WT	WT
ABC DLBCL case #6	Gain/Amp	WT	WT	Y196H	WT	WT
ABC DLBCL case #7	Gain/Amp	WT	Deletion aa191-226	WT	L265P	WT
ABC DLBCL case #8	Gain/Amp	WT	WT	WT	V217F	WT
ABC DLBCL case #9	Gain/Amp	WT	WT	E197G	WT	WT
ABC DLBCL case #10	Gain/Amp	WT	WT	WT	L265P	WT
ABC DLBCL case #11	Gain/Amp	WT	WT	WT	W218R/I220T	WT

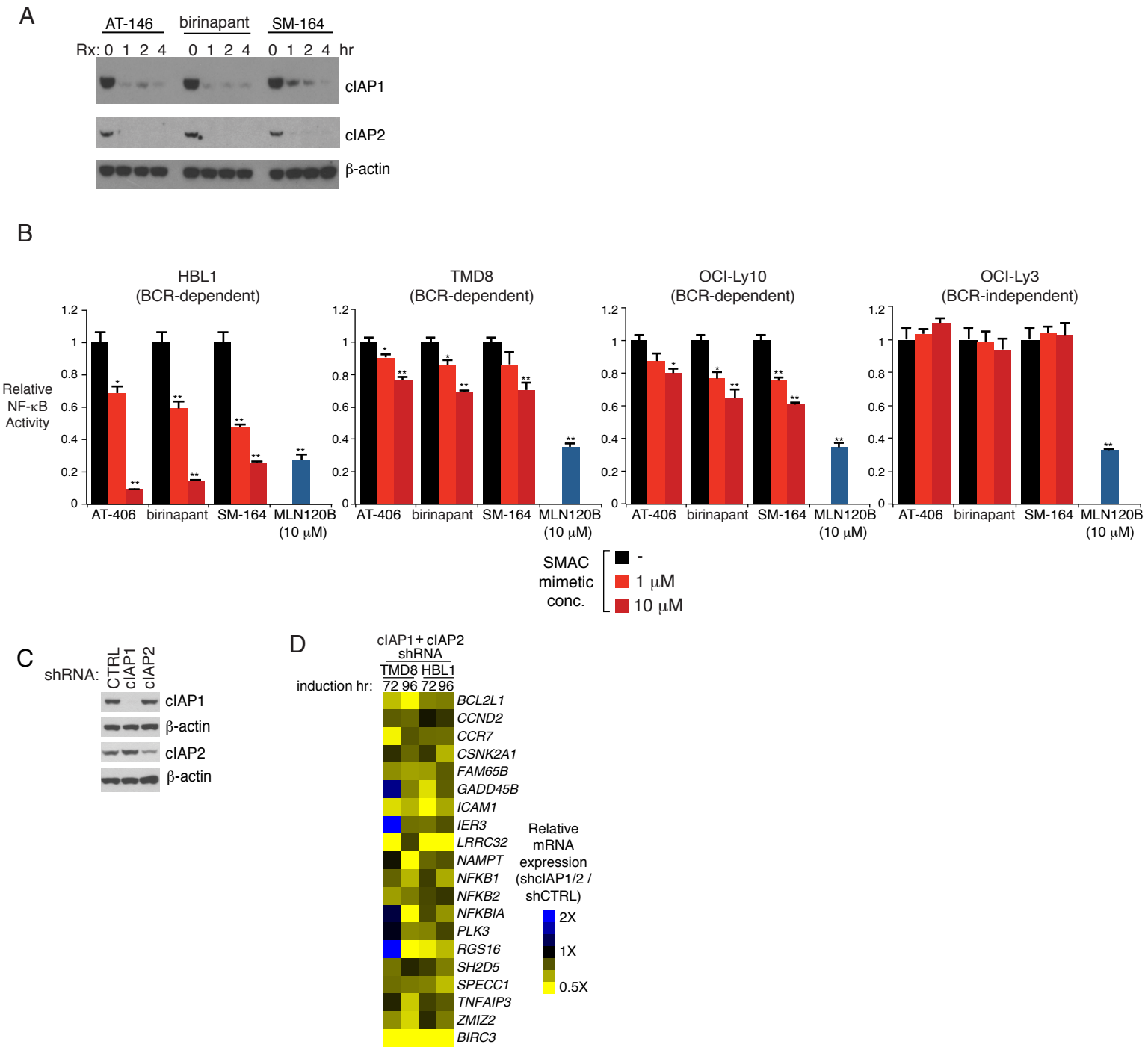

Figure S2, related to Figure 2: cIAP1/2 contribute to the classic NF-κB activation pathway in ABC DLBCL. **(A)** HBL1 ABC DLBCL cells were treated with 3 SMAC mimetics (5 μM) for indicated time. Total cell lysates were analyzed by immunoblotting for the indicated proteins. **(B)** Relative activity of an NF-κB-dependent luciferase reporter in four ABC DLBCL lines (BCR-dependent or BCR-independent) after treatment with the indicated concentrations of 3 SMAC mimetics or the IKKβ inhibitor MLN120B for 24 hours. Error bars denote SEM of triplicates. p values (Student's t test) compare treatment groups with the DMSO control; * $p < 0.05$; ** $p < 0.01$. **(C)** Whole cell lysates from HBL1 ABC DLBCL cells expressing the indicated shRNAs were analyzed by immunoblotting for the indicated proteins. **(D)** Changes in NF-κB signature genes expression in ABC DLBCL cell lines over a time course of cIAP1/2 shRNA induction. Shown are genes that reflect NF-κB activity in ABC DLBCL. Relative mRNA levels are depicted according to the color scale shown.

Table S2, related to Figure 2, is provided as separate Excel files.

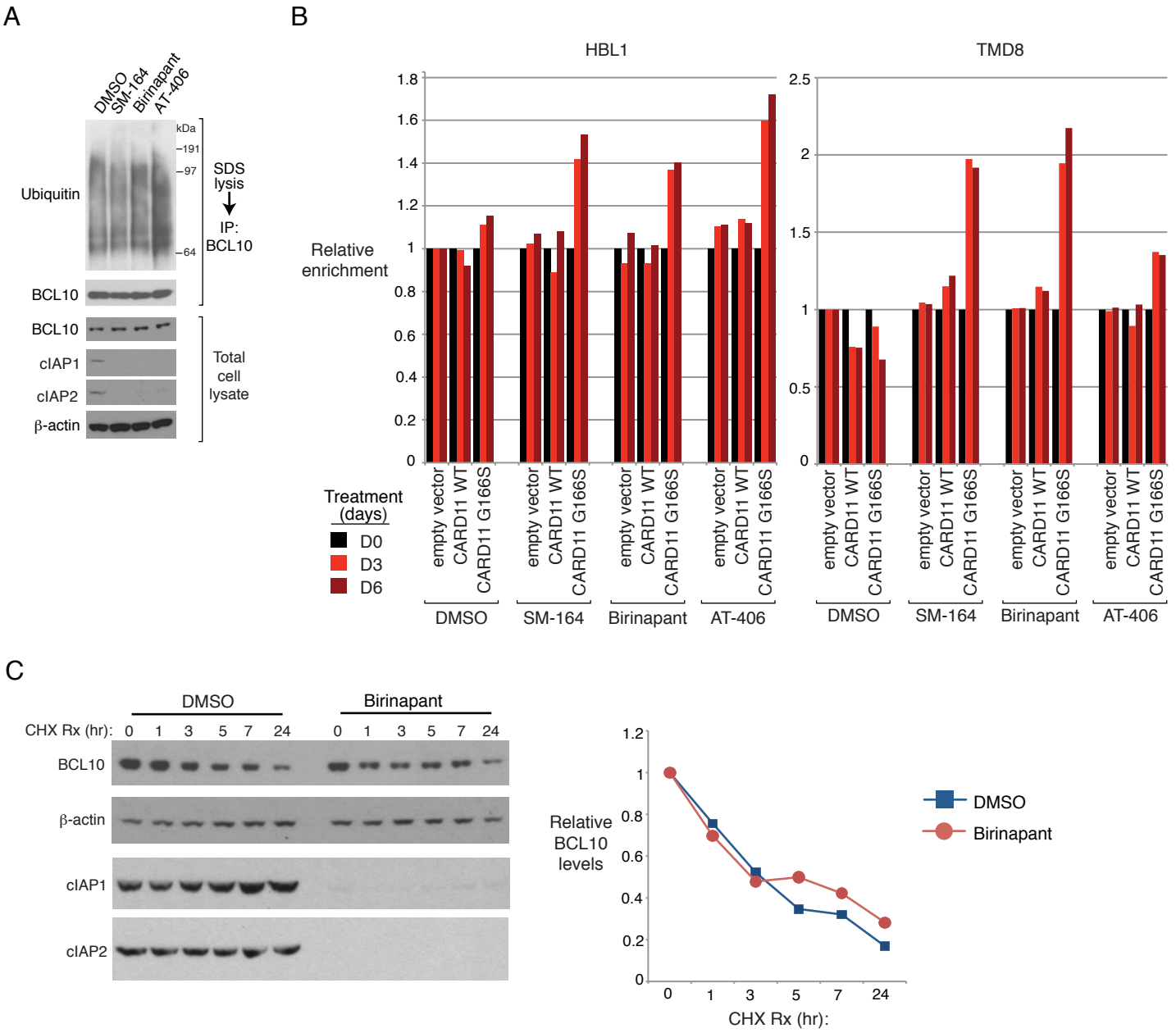

Figure S3, related to Figure 3: cIAP1/2 expression is required for BCL10 K63-specific ubiquitination in CARD11 WT but not in CARD11 mutated ABC DLBCL cells.

(A) SDS (1%) lysates prepared from OCI-Ly3 cells treated with indicated SMAC mimetics (5 μM) for 24 hours were diluted and subjected to anti-BCL10 immunoprecipitation. Immunoprecipitates or total cell lysates were analyzed by immunoblotting for the indicated proteins. **(B)** Viability of ABC DLBCL lines expressing control, CARD11 WT, or CARD11 G166S mutant were treated with DMSO, SM-164 (5 μM), Birinapant (5 μM) or At-406 (5 μM) and analyzed by FACS for viable GFP^{+}/CARD11-expressing cells over a time course, normalized to the day 0 values. **(C)** HBL1 ABC DLBCL cells were pre-treated with DMSO or birinapant for 2 hours, followed by treatment with Cycloheximide (10 μg/ml) for the indicated times. Total cell lysates were prepared and analyzed by immunoblotting for the indicated proteins. The relative BCL10 protein signal intensity was determined by densitometric analysis (right).

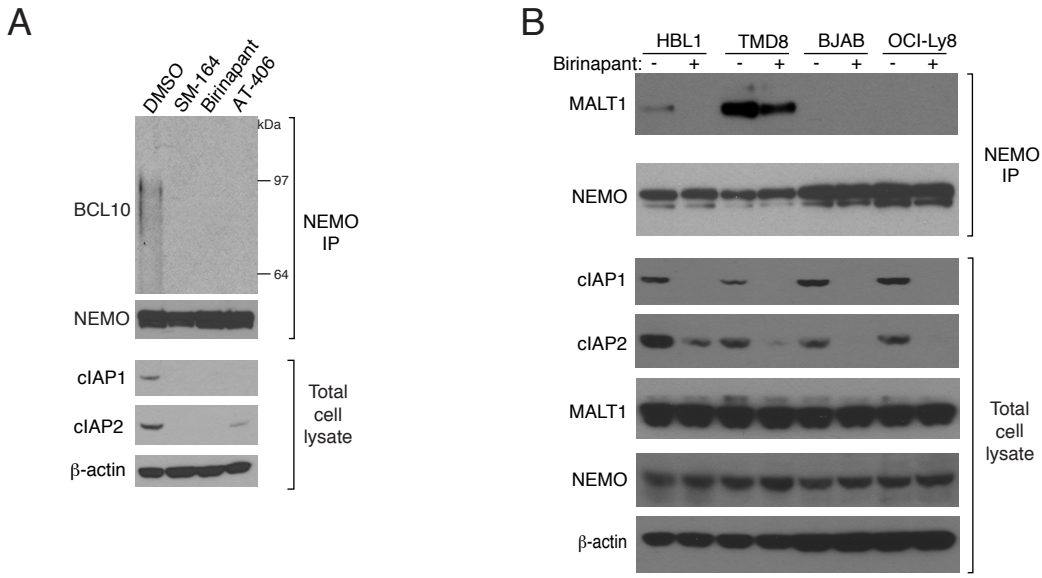

Figure S4, related to Figure 4: The binding of NEMO to CBM complex in ABC DLBCL cells depends on cIAP1/2.

(A) ABC DLBCL line HBL1 was treated with indicated SMAC mimetics (5 μM) for 24 hours and immunoprecipitated with anti-NEMO antibody. Immunopreciptates or total cell lysates were immunoblotted for the indicated proteins. **(B)** DLBCL lines were treated with birinapant (5 μM) for 24 hours. Lysates were prepared and subjected to anti-NEMO immunoprecipitation, followed by immunoblotting for indicated proteins. Lysates were additionally analyzed by immunoblotting for the indicated proteins.

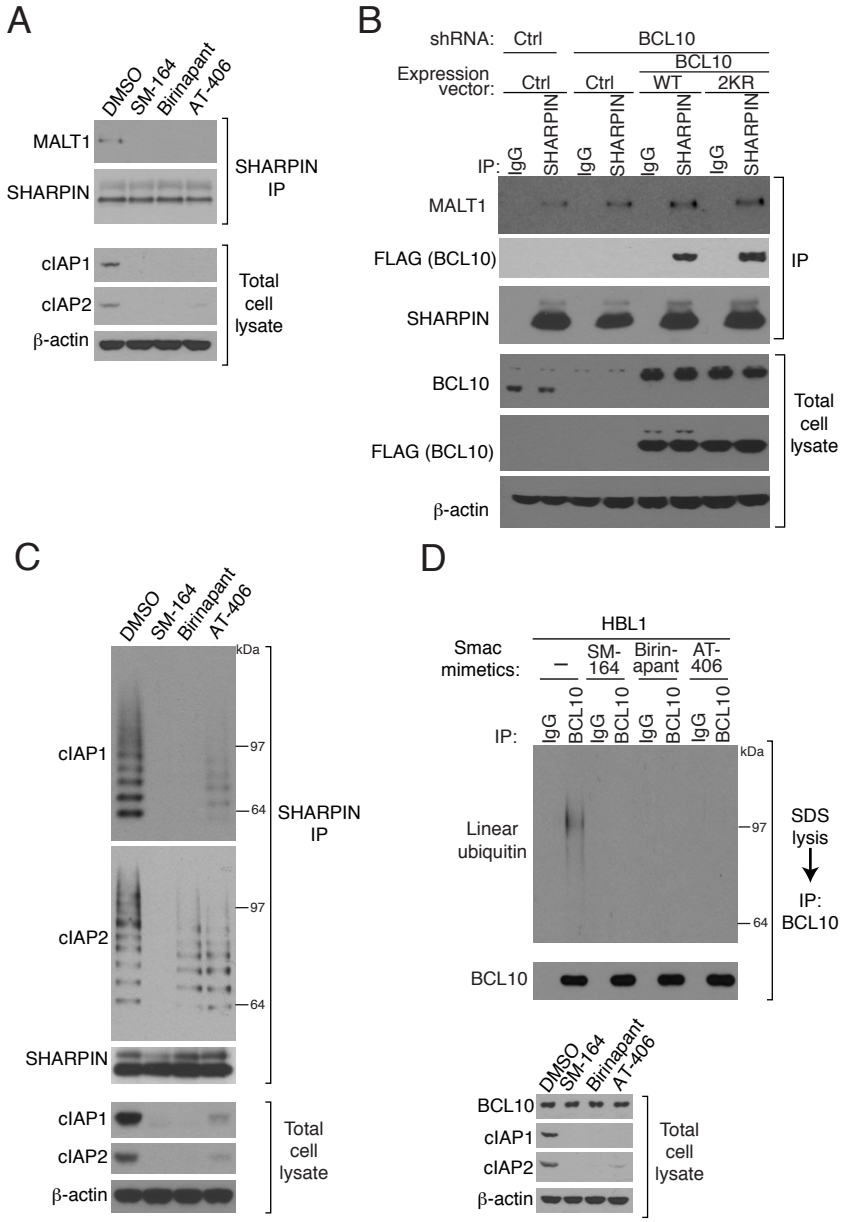

Figure S5, related to Figure 5: LUBAC recruitment to the CBM complex in ABC DLBCL depends on cIAP1/2. **(A)** HBL1 ABC DLBCL cells were treated with indicated SMAC mimetics (5 μM) for 24 hours and subjected to anti-SHARPIN immunoprecipitation. Immunoprecipitates or total cell lysates were immunoblotted for the indicated proteins. **(B)** Control or BCL10 shRNAs were inducibly expressed using retroviral vectors in HBL1 cells that had been transduced with retroviral vectors expressing Flag epitope-tagged WT or 2KR BCL10, or with a control vector. shRNA induced cells were prepared and subjected to anti-SHARPIN immunoprecipitation, followed by immunoblotting for indicated proteins. Lysates were additionally analyzed by immunoblotting for the indicated proteins. **(C)** Lysates prepared from HBL1 cells treated with indicated SMAC mimetics (5 μM) for 24 hours were subjected to anti-SHARPIN immunoprecipitation. Immunoprecipitates or total cell lysates were immunoblotted for the indicated proteins. **(D)** Lysates prepared using 1% SDS from HBL1 ABC DLBCL cells treated with indicated SMAC mimetics (5 μM) for 24 hours were diluted and then subjected to immunoprecipitation with anti-BCL10 antibody or with control IgG. Immunoprecipitates or total cell lysates were immunoblotted for the indicated proteins.

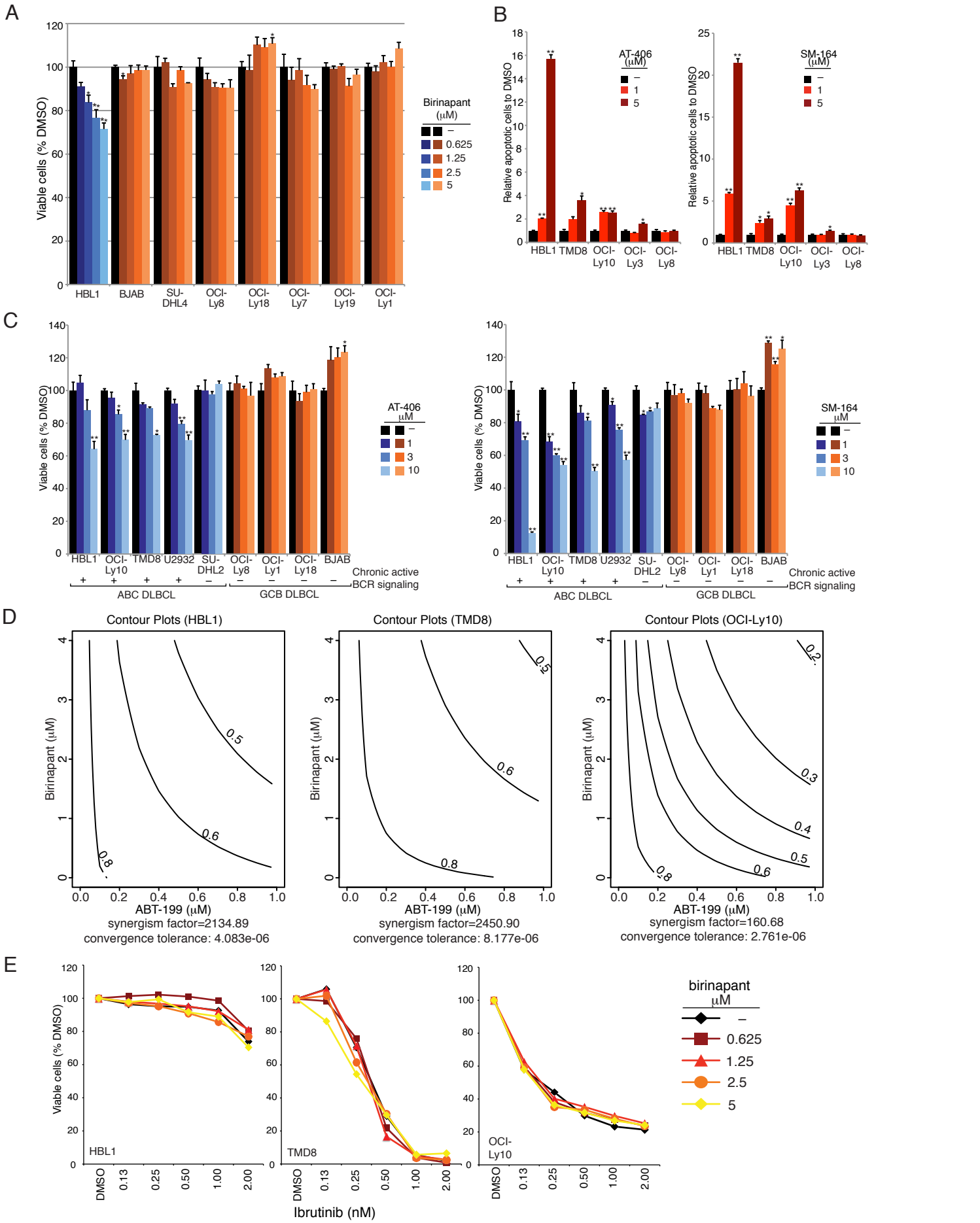
A
Viable cells (% DMSO)
Birinapant (μM)
–
0.625
1.25
2.5
5
HBL1
BJAB
SU-DHL4
OCI-Ly8
OCI-Ly18
OCI-Ly7
OCI-Ly19
OCI-Ly1
B
Relative apoptotic cells to DMSO
AT-406 (μM)
SM-164 (μM)
HBL1
TMD8
OCI-Ly10
OCI-Ly3
OCI-Ly8
C
Viable cells (% DMSO)
AT-406 μM
SM-164 μM
–
1
3
10
U2932
SU-DHL2
OCI-Ly18
Chronic active BCR signaling
ABC DLBCL
GCB DLBCL
D
Contour Plots (HBL1)
Contour Plots (TMD8)
Contour Plots (OCI-Ly10)
Birinapant (μM)
ABT-199 (μM)
synergism factor=2134.89
convergence tolerance: 4.083e-06
synergism factor=2450.90
convergence tolerance: 8.177e-06
synergism factor=160.68
convergence tolerance: 2.761e-06
E
Viable cells (% DMSO)
birinapant μM
Ibrutinib (nM)
DMSO
0.13
0.25
0.50
1.00
2.00

Figure S6, related to Figure 6: SMAC mimetic drugs are selectively toxic for BCR-dependent ABC DLBCL lines.

(A) Viability of the indicated DLBCL lines treated with birinapant at the indicated concentrations for 5 days, normalized to DMSO-treated cells. **(B)** Relative apoptotic cells, measured by cleavage of PARP and Caspase 3, in DLBCL lines treated with AT-406 or SM-164 at the indicated concentrations for 2 days, normalized to DMSO-treated cells. **(C)** Viability of the indicated DLBCL lines treated with AT-406 or SM-164 at the indicated concentrations for 5 days, normalized to DMSO-treated cells. Dependence of each line on BCR signaling is indicated. **(D)** Formal calculation of synergism between ABT-199 and birinapant. The raw cell viability data from Figure 7C was entered into an S-plus program developed based on the method in (Greco et al., 1990). The resulting contour plots; the synergism-antagonism factor, and the convergence tolerance are shown. High positive synergism-antagonism factor values indicate strong synergy. **(E)** Viability of ABC DLBCL lines after treatment for 4 days with the indicated concentrations of birinapant, the BTK inhibitor ibrutinib, or birinapant + ibrutinib. Data are normalized to DMSO-treated cells, and then to cells treated with birinapant alone. Error bars denote SEM of triplicates. p value was calculated using Student's t test comparing treatment groups with DMSO control; * indicates $p < 0.05$; ** indicates $p < 0.01$.

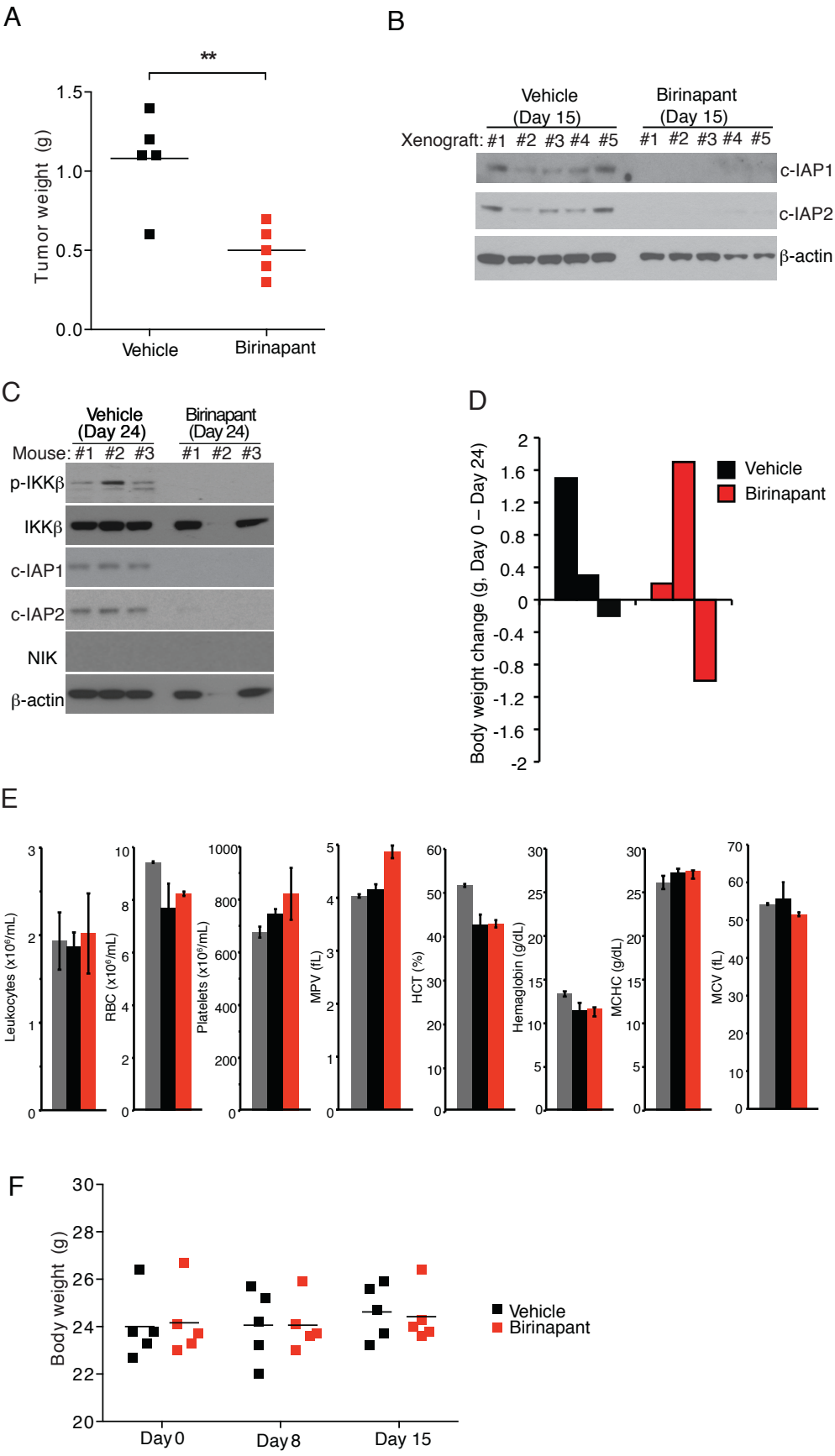
A
**
Tumor weight (g)
1.5
1.0
0.5
0.0
Vehicle
Birinapant
B
Vehicle (Day 15)
Birinapant (Day 15)
Xenograft: #1 #2 #3 #4 #5 #1 #2 #3 #4 #5
c-IAP1
c-IAP2
β-actin
C
Vehicle (Day 24)
Birinapant (Day 24)
Mouse: #1 #2 #3 #1 #2 #3
p-IKKβ
IKKβ
c-IAP1
c-IAP2
NIK
β-actin
D
Body weight change (g, Day 0 – Day 24)
2
1.6
1.2
0.8
0.4
0
-0.4
-0.8
-1.2
-1.6
-2
Vehicle
Birinapant
E
Leukocytes (x10⁶/mL)
RBC (x10⁶/mL)
Platelets (x10⁶/mL)
MPV (fL)
HCT (%)
Hemaglobin (g/dL)
MCHC (g/dL)
MCV (fL)
Untreated
Vehicle
Birinapant
F
Body weight (g)
30
28
26
24
22
20
Day 0
Day 8
Day 15
Vehicle
Birinapant

Figure S7, related to Figure 7: Birinapant inhibits mice xenograft models of ABC DLBCL in vivo.

(A) Tumor weight of DLBCL2 xenografts from NOD/SCID mice after 15-day treatment with either birinapant (30 mg/kg; three times per week) or vehicle. Horizontal bars indicate the mean (n=5 mice). p values (Student's t test) compare the vehicle and birinapant groups; ** $p < 0.01$. **(B)** Human tumor cells were purified from DLBCL2 xenografts (see Experimental Procedures) at the endpoint of birinapant treatment (30 mg/kg; three times per week), and total cell lysates were analyzed by immunoblotting for the indicated proteins. **(C)** Human tumor cells were purified from HBL1 xenografts (see Experimental Procedures) at the endpoint of treatment in Figure 7D, and total cell lysates were analyzed by immunoblotting for the indicated proteins. The tumor from birinapant-treated mouse #2 was very small and yielded insufficient protein for analysis. **(D)** Body weight change in NOD/SCID mice carrying HBL1 tumors, following 24 day treatment with birinapant (30 mg/kg; TIW) or vehicle. Body weight was measured at day 0 and day 24, and the change in weight is shown. **(E)** Blood cell parameters from NOD/SCID mice carrying HBL1 tumors following treatment with either birinapant (30 mg/kg; three times per week) or vehicle for 24 days. Blood was obtained via cardiac puncture from mice 24 hours post-final birinapant or vehicle treatment. The indicated blood cell parameters were determined using the MASCOT Hematology Profile on an automated Hemavet 950 FS analyzer (Drew Scientific Group). Untreated NOD/SCID mice served as a control for baseline blood cell parameters. Data indicate the mean ± SEM (n=3 mice). No statistically significant differences were determined. **(F)** Body weight of individual NOD/SCID mice carrying DLBCL2 xenografts, following treatment with either birinapant (30 mg/kg; TIW) or vehicle. Body weight was measured at the indicated time points of treatment. No statistically significant differences were found between birinapant and vehicle treatment groups. Horizontal bars indicate the mean (n=5 mice).

Supplemental Experimental Procedures

Patient samples. Tumor biopsy specimens prior to treatment were obtained from patients with de novo DLBCL, which were previously classified by gene expression profiling. The normal genomic samples were from peripheral blood mononuclear cells of health donors. DNA from patient samples was extracted with the DNeasy Tissue kit (Qiagen) according to the manufacturer's instructions.

***BIRC2* and *BIRC3* copy number and gene expression analysis.** The R package aroma.affymetrix (Bengtsson et al., 2008) was used to pre-process the Affymetrix 250k-Sty SNP array data (.CEL files). The subtype classification (ABC and GCB) of 128 DLBCL cases was extracted from the GEO meta data. The GLAD method (Gain and Loss Analysis of DNA. R package version 2.30.0.) was used for calling segment copy numbers. Genome positions of *BIRC2* and *BIRC3* were used to extract sample copy numbers for these two genes. The R Bioconductor (Gentleman et al., 2004) and affy package (Gautier et al., 2004) was used to process the raw Affymetrix GeneChip Human Genome U133A microarray data. Normalization was done using the RMA method (Bolstad et al., 2003). The annotation based on the R hgu133a.db package was used to extract expression values of the *BIRC2* and *BIRC3* genes. The R language was used to calculate and plot correlation of gene expression levels with copy number for *BIRC2* and *BIRC3*. The correlation of the gene expression of *BIRC2* and *BIRC3* in U133A microarray with the relative copy number was plotted. Copy number 0 means no copy number changes (N=2).

Samples for Affymetrix SNP6.0 array analysis were processed with the standard Affymetrix protocol for the Genome-Wide Human SNP Nsp/Sty 6.0 array (Affymetrix Genome-Wide Human SNP Nsp/Sty 6.0 User Guide, rev 8), using the isopropanol precipitation PCR purification option. Signal copy values for individual probes were generated using Aroma Affymetrix algorithm (Bengtsson et al., 2008), as implemented in the CRAN library (https://cran.r-project.org/web/packages/aroma.affymetrix/). Based on these signal values, the chromosomes of a given sample were divided into segments of

similar signal value, each of which was assigned to one of 5 categories (homozygous deletion, heterozygous deletion, wild- type, single copy gain, amplification) according to previously described methods (Lenz et al., 2008b). The genomic coordinates on chromosome 11 in Figure 1D are based on human genome build 37 (hg19).

Cell Culture. The DLBCL cell lines BJAB, SUDHL4, HBL1, DLBCL2, TMD8, U2932, SUDHL2, and YM were grown in RPMI-1640 medium (Invitrogen) +10%FBS (Hyclone, Defined) +pen/strep (Invitrogen); the cell lines OCI-Ly3, OCI-Ly10, OCI-Ly7, OCI-Ly8, OCI-Ly1 and OCI-Ly19 cell lines were grown in IMDM medium (Invitrogen) +20% human serum +pen/strep (Invitrogen). All cell lines were grown to log phase at 37^{o}C, 5% CO_2 when experiments started.

Real-Time Quantitative PCR. Real-time quantitative PCR was used to evaluate copy number alterations detected by array CGH as described previously (Bea et al., 2005) (Rosenwald et al., 2003) (Ngo et al., 2011). The genomic copy number of BIRC3 was determined relative to the control genes *CHMP4A*, which is not subject to copy number alterations in ABC DLBCL. To determine the cut-off values for a genomic gain/amplification, 6 DNA samples from peripheral blood of healthy individuals were studied. The following quantitative PCR primers were used: CHMP4A-F, 5′-GGCATTGTTGCGTGATTTCTTAGC-3′ (qPCR control gene); CHMP4A-R, 5′-AGAAATGGCATCTGAGATCTGCTG-3′ (qPCR control gene); BIRC3-F, 5′-GTTCTCTGACCCAACCCAGA-3′ (qPCR BIRC3); BIRC3-R, 5′-GAGCAATTGTTGGCTGATGA-3′ (qPCR BIRC3);

Gene expression profiling: Gene expression profiling was performed using two-color human Agilent 4x44K gene expression arrays, exactly as described by the manufacturer, comparing signal from control cells (Cy3) and experimentally manipulated cells (Cy5). Array elements were filtered for those meeting confidence thresholds for spot size, architecture, and level above local background. These criteria are a feature of the Agilent gene expression software package for Agilent 4x44k arrays.

Antibodies and reagents. The antibodies used in this study were purchased as follows: anti-IKKβ, anti-phospho-IKKβ, anti-IκBα, anti-phospho-IκBα, anti-cIAP1, anti-NIK from Cell Signaling Technologies; anti-cIAP2 from BD Pharmingen; anti-ubiquitin (VU-1), anti-linear ubiquitin (LUB9) from Life Sensors; polyclonal anti-NEMO/IKKγ (FL−419), anti-β-actin, anti-IRAK1, anti-MALT1, anti-BCL10 from Santa Cruz Biotechnology; monoclonal anti-NEMO/IKKγ, anti-MALT1, anti-BCL10 and anti-CD79A from Santa Cruz Biotechnology; anti-SHARPIN from BETHYL; anti-FLAG-tag from Sigma; anti-human IgM from Jackson ImmunoResearch Lab. Isotype control antibodies were obtained from the same company as each experimental antibody. Secondary HRP-conjugated antibodies were obtained from GE Healthcare.

The SMAC mimetics compounds AT-406, birinapant, SM-164 and NIK inhibitor were from the National Center for Advancing Translational Sciences (NCATS). The BCL2 inhibitor ABT-199 was obtained from selleckchem. The IKKβ inhibitor MLN120B was obtained from Millennium Pharmaceuticals. The BTK inhibitor (ibrutinib) was obtained from Pharmacyclics, Inc. Tissue culture grade DMSO vehicle control was obtained from Sigma-Aldrich.

Immunoblotting. Cell pellets were lysed in the modified RIPA buffer (50mM Tris-HCl pH 7.5, 150mM NaCl, 1% NP40, 0.25% deoxycholic acid, 1mM EDTA) supplemented with protease inhibitor tablet and phosphatase inhibitor tablet (Roche), 1mM DTT, 1mM Na_3VaO_4, 1mM PMSF. Protein concentration was measured by BCA Protein Assay Kit (Thermo Scientific). Total proteins were separated on 4% to 12% SDS-polyacrylamide gels and transferred to nitrocellulose membranes.

BCL10/NEMO immunoprecipitation and ubiquitination analysis. For BCL10 ubiquitination, cells were boiled 15 minutes in 1% SDS before immunoprecipitation. Boiled lysates were diluted to 0.1% SDS with a modified RIPA buffer (50mM Tris-HCl pH 7.5, 150mM NaCl, 1% NP40, 0.25% deoxycholic acid, 1mM EDTA, supplemented with protease inhibitors and 5mM N-ethylmaleimide (Sigma)). Cleared lysates were incubated overnight with polyclonal anti-BCL10 antibody (Santa Cruz H-197). Immunoprecipitates were washed 5 times with lysis buffer, separated by SDS-PAGE,

transferred to nitrocellulose and analyzed by immunoblotting with an anti-ubquitin antibody (VU-1).

The method for the detection of BCL10/NEMO linear polyubiquitination was described (Tokunaga et al., 2011). In brief, cells were boiled 15 mins in 1% SDS then diluted to 0.1% SDS with a modified RIPA buffer. Cleared lysates were subjected to immunoprecipitation with polyclonal anti-NEMO/IKKγ antibody (Santa Cruz FL–419) or anti-BCL10 antibody (Santa Cruz H-197). Immunoprecipitates were separated on 4% to 12% SDS-polyacrylamide gels and transferred to nitrocellulose membranes, autoclaved with distilled water at 121 degree for 30 min, and then autoclaved again for 15 min without water. Membranes were analyzed by immunoblotting with an anti–linear ubiquitin antibody (LUB9).

Co-immunoprecipitation. Cells were lysed in an endogenous lysis buffer (20mM Tris-HCl pH 7.6, 150mM NaCl, 1mM EDTA, 1% Triton X-100, 30mM NaF, and 2mM sodium pyrophosphate) supplemented with complete protease inhibitor cocktail (Roche), phosphatase inhibitor tablet (Roche), 1mM DTT, 1mM Na_3VaO_4, 1mM PMSF. Cleared lysates were incubated overnight with polyclonal anti-MALT, anti-IRAK1, ant-SHARPIN and control antibodies. Immunoprecipitates were washed 5 times with 0.5M NaCl lysis buffer, separated by SDS-PAGE, transferred to nitrocellulose and analyzed by immunoblotting.

Tandem Ubiquitin Binding Entities (TUBEs) assay. Biotin labeled K63 and K48 specific Tandem Ubiquitin Binding Entities (TUBEs) were obtained from *LifeSensors.* To measure K63 or K48 specific protein ubiquitination in DLBCL cells, cells were boiled 30 mins in 1% SDS then diluted to 0.1% SDS with a modified RIPA buffer. Cleared lysates were subjected to incubation with K63 or K48 specific Tandem Ubiquitin Binding Entities (TUBEs) overnight, and then purified with streptavidin beads. Immunoprecipitates were separated by SDS-PAGE, transferred to nitrocellulose and analyzed by immunoblotting with anti-BCL10, anti-cIAP1 or anti-cIAP2 antibodies.

NF-κB family subunits DNA-binding ELISA. NF-κB family subunits DNA-binding

activity was measured using TransAM NF-κB Transcription Factor ELISA Kits obtained from Active Motif, following manufacturer's instructions. In brief, an oligonucleotide containing the NF-κB consensus site (5′-GGGACTTTCC-3′) has been immobilized in a 96-well plate. The activity of NF-κB subunits contained in nuclear extract was measured by the binding ability to this oligonucleotide. The p65, p50, p52, c-Rel or RelB antibodies are accessible only when the corresponding NF-κB subunits is activated and bound to its target DNA.

IκB kinase activity reporter assay. The assay for IκB kinase activity using the IκBα-photinus luciferase reporter has been described (Lenz et al., 2008a). In brief, stable clones of TMD8 were constructed with vectors to express a fusion protein between IκBα and Photinus luciferase (from pGL3; Promega) as the reporter, and Renilla luciferase (from phRL-TK; Promega) for normalization. The ratio of IκBα –Photinus to Renilla luminescence was measured by Dual- Glo luciferase assay system (Promega), and was normalized to that in untreated controls.

NF-κB reporter assays. NF-κB transcriptional reporter ABC DLBCL lines were generated by transduction with lentiviral particles containing an inducible NF-κB responsive luciferase reporter construct (SA Biosciences) and selected with puromycin. Luciferase activity was measured using the Dual-Luciferase Reporter Assay System (Promega).

Cell viability (MTS) assay. Cells were plated in triplicate at a density of 10,000 cells per well in 96-well plates. Cell viability after indicated treatments was assayed by adding MTS reagents (Promega), incubated for 1h and measured by the amount of 490nm absorbance using a 96-well plate reader. The background was subtracted using a media only control.

Apoptosis measurement. The activation of programmed cell death was measured by intracellular flow cytometry methods (Sciammas et al., 2006) using antibodies against

cleaved (activated) caspase-3 (PE, Becton-Dickenson) and cleaved PARP (APC, Becton-Dickenson), according to the manufacturer's instructions.

Retroviral vectors and transduction for expression in lymphoma cells. The retroviral vectors for shRNA expression were described before (Ngo et al., 2011). Sequences for control and target specific shRNAs are as following: Control shRNA (CTCTCAACCCTTTAAATCTGA); cIAP1 shRNA (TAGTCTGCTTTGGTACTAATA); cIAP2 shRNA (GCCCTCTAGTGTTCTAGTTAA); NIK shRNA (GGTGTGAAAGTCCAAATACAG); IKKα shRNA (GGTGGAAAGATAATACATAAA); RELB shRNA (GCCATTGCCTTTCACGTACCT); NEMO shRNA (GGCCACTGCCTGCCGAGGACG); BCL10 shRNA (CTGACATTGTCTCCTATATAT). Human BCL10 and NEMO constructs were provided by Dr. Jonathan D. Ashwell, (National Cancer Institute, National Institutes of Health, Bethesda, MD) and were described (Wu and Ashwell, 2008). CARD11 wild type and G166S constructs were described in (Lenz et al., 2008a).

Purification of cIAP1 and cIAP2 double knockdown cells. Retroviral constructs for shRNA expression are described (Lenz et al., 2008c; Shaffer et al., 2008). For cIAP2 shRNA, the puromycin selectable marker is replaced by a puro-GFP fusion gene for tracking by flow cytometry. For cIAP1 shRNA, the puromycin selectable marker is replaced by a Lyt2/CD8a gene for tracking by flow cytometry and purification. For double knockdown purification, double infected cells were first selected with puromycin, recovered, and then secondary purified with the mouse CD8 (Lyt2) Dynabeads (Invitrogen, Catalog # 11447D).

LentiCRISPR and transduction for expression in lymphoma cells. Lentiviral expression vector for Cas9 and sgRNA (lentiCRISPR) was descripted (Shalem et al., 2014). For lymphoma transduction, sgRNA constructs were mixed with the packaging and envelope plasmid psPAX2 and pMD2.G and were transfected into 293T cells using the Lipofectamine 2000 reagent (Invitrogen). The produced lentiviral was concentrated using Lenti-*X*™ Concentrator (Clontech), and was used to infect lymphoma cells in the presence of 8mg/ml polybrene in a single spin infection. Puromycin was used to select

for stable integrants over 12 days. Sequences for control and target specific sgRNAs are as following: AAVS1/Control sgRNA (GGGGCCACTAGGGACAGGAT); cIAP1 #1 sgRNA (CATGGGTAGAACATGCCAAG); cIAP1 #2 sgRNA (GAGTTCTTGATACGAATGAA); cIAP2 #1 sgRNA (CCTACCTGTTCAAGTAGATG); cIAP2 #2 sgRNA (GACTCTGCATTTTCATCTCC); cIAP2 #3 sgRNA (CTATCCACATCAGACAGCCC).

Tumor model and therapy study: To establish tumor xenografts, $2x10^6$ HBL1 cells, and $5x10^6$ DLBCL2 cells were inoculated into the right flank of female NOD/SCID mice (NCI-Frederick, Frederick, MD). Cells were administered in a 1:1 solution of PBS and Matrigel. Tumor growth was monitored by measuring tumor size in two orthogonal dimensions, using digital calipers. Tumor volume was calculated using the formula (long dimension/2) x (short dimension)^2. For the birinapant treatment schedule, mice were administered 30 mg/kg/day birinapant (in 200 μL volume) by intraperitoneal injection three times per week (i.e. on Monday, Wednesday and Friday). Birinapant was formulated in 12.5% Captisol® (Cydex Pharmaceuticals, Kansas) vehicle solution. Vehicle was formulated by slowly adding Captisol® to sterile water, and stirring rapidly until dissolved (25 g/200 mL). The pH was adjusted to 4.0 whilst mixing on low speed.

Supplemental References

Bea, S., Zettl, A., Wright, G., Salaverria, I., Jehn, P., Moreno, V., Burek, C., Ott, G., Puig, X., Yang, L.*, et al.* (2005). Diffuse large B-cell lymphoma subgroups have distinct genetic profiles that influence tumor biology and improve gene-expression-based survival prediction. Blood *106*, 3183-3190.

Rosenwald, A., Wright, G., Wiestner, A., Chan, W. C., Connors, J. M., Campo, E., Gascoyne, R. D., Grogan, T. M., Muller-Hermelink, H. K., Smeland, E. B.*, et al.* (2003). The proliferation gene expression signature is a quantitative integrator of oncogenic events that predicts survival in mantle cell lymphoma. Cancer Cell *3*, 185-197.

Sciammas, R., Shaffer, A. L., Schatz, J. H., Zhao, H., Staudt, L. M., and Singh, H. (2006). Graded expression of interferon regulatory factor-4 coordinates isotype switching with plasma cell differentiation. Immunity *25*, 225-236.

Shaffer, A. L., Emre, N. C., Lamy, L., Ngo, V. N., Wright, G., Xiao, W., Powell, J., Dave, S., Yu, X., Zhao, H.*, et al.* (2008). IRF4 addiction in multiple myeloma. Nature *454*, 226-231.

Tokunaga, F., Nakagawa, T., Nakahara, M., Saeki, Y., Taniguchi, M., Sakata, S., Tanaka, K., Nakano, H., and Iwai, K. (2011). SHARPIN is a component of the NF-kappaB-activating linear ubiquitin chain assembly complex. Nature *471*, 633-636.